NTNU – Trondheim
Norwegian University of
Science and Technology

Obtaining the Source Wavefield from Multicomponent Data and its Application in Full Waveform Inversion

Uno Brosten Vaaland

Petroleum Geoscience and Engineering
Submission date: June 2015
Supervisor: Børge Arntsen, IPT

Norwegian University of Science and Technology
Department of Petroleum Engineering and Applied Geophysics

Obtaining the Source Wavefield from Multicomponent Data and its Application in Full Waveform Inversion

*Uno Brosten Vaaland**

ABSTRACT

In full waveform inversion (FWI) we need to know the seismic source signature. In practice this is generally unknown, and it must be estimated using statistical methods or inversion. However, these methods rely on assumptions that are often false, which results in a poorly estimated source. This can have a crippling effect on FWI, since it is an ill-posed and highly nonlinear problem that is very sensitive to errors in the inputs. Small errors in the source can cause the solution predicted by FWI to deviate significantly from the true solution. To better estimate the source for FWI, we suggest using a method for extracting the source wavefield when given multicomponent data. The method for obtaining the source wavefield derives from the reciprocity theorem, and involves injecting the multicomponent data into an homogeneous model with a finite difference injector. We then use the source wavefield as input for the source in FWI. Numerical examples are presented, and we find that the extracted source field can successfully be used in FWI, although numerical inaccuracies inhibits it from fulfilling its true potential.

INTRODUCTION

Full waveform inversion (FWI) is a method for fitting a model to the observed data by considering the full waveform in the optimization (Virieux and Operto, 2009). It is an ill-posed problem that is highly nonlinear, and therefore it requires some regularization and preconditioning to better constrain the inversion process (Aster and Thurber, 2013). Part of the preconditioning involves knowing the seismic source signature, which is generally unknown and is considered an unknown in the inversion problem (Pratt, 1999). Therefore, it necessary to estimate the source signature. This can be done using statistical methods, or by inverting for the source. However, the statistical methods are based on assumptions that are generally false in practice (Ziolkowski, 1991), and inverting for the source only gives a good solution if the predicted model is close to the true model (Pratt, 1999). Having an inaccurate source input has a great impact on the result. Full waveform inversion is very sensitive to error in the inputs, and small errors may cause the best fitting model to deviate significantly from the true model. Therefore, it is of great importance that we accurately know the source input if we want the full waveform inversion to give a useful result.

In this work we want to better estimate the source by extracting the source wavefield from multicomponent data and using this as input in full waveform inversion. The method we use is similar to the method presented by Amundsen and Robertsson (2014) and it makes it

*Department of Petroleum Engineering & Applied Geophysics, Norwegian University of Science and Technology, Trondheim, Norway

possible to obtain the original source wavefield, when given multicomponent seismic data. The method is based on the reciprocity theorem and works by injecting the multicomponent data into a homogeneous medium. We present numerical experiments that show how we successfully obtain the source wavefield, and how it can be used as source in full waveform inversion. The result is compared with a benchmark inversion result that was generated using the same point source as the multicomponent data was generated with. We find that the extracted source field can successfully be used in FWI, although numerical inaccuracies inhibits it from fulfilling its true potential.

This work is organized into two parts. In the first part, we derive the theory behind the method for extracting the source wavefield by injecting multicomponent data. Then, we provide numerical examples that show how the method works, and perform a sensitivity analysis. In the second part, we give a brief description of full waveform inversion, and then we show a numerical experiment where we use the extracted source wavefield as the source input in full waveform inversion.

PART I:
Obtaining The Source Wavefield

WAVE THEORY

Definitions

- c is the subsurface velocity model function. For each point in the subsurface:

$$\begin{aligned} c : V &\mapsto \mathbb{R} \\ \mathbf{x} &\mapsto c(\mathbf{x}), \end{aligned} \tag{1}$$

  where $c(\mathbf{x})$ has units m/s and $V \subset \mathbb{R}^3$ is the area of interest. It is assumed that $c(\mathbf{x})$ does not vary with time.

- p is the pressure field function. It is the pressure value at a given time t, and location $\mathbf{x}$ in the subsurface.

$$\begin{aligned} p : V \times \mathbb{R} \times \mathcal{F}(V, \mathbb{R}) &\mapsto \mathbb{R} \\ (\mathbf{x}, t; c) &\mapsto p(\mathbf{x}, t; c), \end{aligned} \tag{2}$$

  where $p(\mathbf{x}, t; c)$ has units Pa, and $\mathcal{F}(V, \mathbb{R})$ is the set of functions that map V to $\mathbb{R}$. From here on, we will refer to $p(\mathbf{x}, t; c)$ as $p(\mathbf{x}, t)$.

- u is the particle displacement function. It is the displacement of a particle at a given time t, and location $\mathbf{x}$ in the subsurface.

$$u : V \times \mathbb{R} \times \mathcal{F}(V, \mathbb{R}) \mapsto \mathbb{R} \qquad (3)$$
$$(\mathbf{x}, t; c) \mapsto u(\mathbf{x}, t; c),$$

where $u(\mathbf{x}, t; c)$ has units m, and $\mathcal{F}(V, \mathbb{R})$ is the set of functions that map V to $\mathbb{R}$. As for the pressure, we will use $u(\mathbf{x}, t)$ to refer to $u(\mathbf{x}, t; c)$.

- s is the seismic source function:

$$s : V \times \mathbb{R} \mapsto \mathbb{R} \qquad (4)$$
$$(\mathbf{x}, t) \mapsto s(\mathbf{x}, t),$$

where $s(\mathbf{x}, t)$ has units Pa/m^2.

- ρ is the mass density of the medium volume:

$$\rho : V \mapsto \mathbb{R} \qquad (5)$$
$$\mathbf{x} \mapsto \rho(\mathbf{x}),$$

where $\rho(\mathbf{x})$ has units kg/m^3. In this work, we let ρ be constant in V. We denote constant density with subscript zero, ρ_0.

- κ is the bulk modulus of the medium volume:

$$\kappa : V \mapsto \mathbb{R} \qquad (6)$$
$$\mathbf{x} \mapsto \kappa(\mathbf{x}),$$

where $\kappa(\mathbf{x})$ has units Pa.

The Acoustic Wave Equation

To derive the acoustic wave equation that is satisfied by p in an isotropic, constant density medium $\forall \mathbf{x} \in V$ and $\forall t \in \mathbb{R}$, we use Newton's second law (7) together with Hooke's law (8). Consider the case with a source I, located at $\mathbf{x}'$ that is initiated at time t'.

$$\rho_0 \frac{\partial^2 u(\mathbf{x}, t, \mathbf{x}', t')}{\partial t^2} = \nabla p(\mathbf{x}, t, \mathbf{x}', t') \qquad (7)$$

$$p(\mathbf{x}, t, \mathbf{x}', t') = \kappa(\mathbf{x}) \nabla u(\mathbf{x}, t, \mathbf{x}', t') + I(\mathbf{x}', t') \qquad (8)$$

By taking the second order time derivative of equation (8) and inserting equation (7), we get an expression for the acoustic wave equation that is satisfied by p for a constant, isotropic medium $\forall \mathbf{x} \in V$ and $\forall t \in \mathbb{R}$.

$$\frac{1}{c(\mathbf{x})^2}\frac{\partial^2 p(\mathbf{x},t,\mathbf{x}',t')}{\partial t^2} - \nabla^2 p(\mathbf{x},t,\mathbf{x}',t') = s(\mathbf{x}',t') \tag{9}$$

where $s(\mathbf{x}',t') = \ddot{I}(\mathbf{x}',t')$ is the second order time derivative of the original source I and $c(\mathbf{x}) = \sqrt{\kappa(\mathbf{x})/\rho_0}$ is the velocity.

Perturbed Medium

The acoustic wave equation in (9) is for a constant, isotropic medium. That is, a medium with no velocity perturbation. In case of a medium with a velocity perturbation, the expression must be slightly altered. Let c_0 be the unperturbed velocity model, and Δc be a velocity perturbation, such that $c = c_0 + \Delta c$ is the perturbed medium. Then, equation (9) for the unperturbed medium becomes

$$\frac{1}{c_0^2}\frac{\partial^2 p(\mathbf{x},t,\mathbf{x}',t')}{\partial t^2} - \nabla^2 p(\mathbf{x},t,\mathbf{x}',t') = s(\mathbf{x}',t') \tag{10}$$

and for the perturbed medium:

$$\frac{1}{(c_0 + \Delta c(\mathbf{x}))^2}\frac{\partial^2 p(\mathbf{x},t,\mathbf{x}',t')}{\partial t^2} - \nabla^2 p(\mathbf{x},t,\mathbf{x}',t') = s(\mathbf{x}',t') \tag{11}$$

If we assume that the model perturbation is small compared to the background (c_0), $|\Delta c(\mathbf{x})| \ll |c_0|$, then we can use the following expansion:

$$\frac{1}{(c_0 + \Delta c(\mathbf{x}))^2} \approx \frac{1}{c_0^2}\left(1 - \frac{2\Delta c(\mathbf{x})}{c_0}\right) \tag{12}$$

We then let $\alpha(\mathbf{x}) = -2\Delta c(\mathbf{x})/c_0$ and write

$$\frac{1}{c(\mathbf{x})^2} = \frac{1}{c_0^2}(1 + \alpha(\mathbf{x})) \tag{13}$$

Substituting this result into equation (11) yields the following expression for the acoustic wave equation for the perturbed medium:

$$\frac{(1 + \alpha(\mathbf{x}))}{c_0^2}\frac{\partial^2 p(\mathbf{x},t,\mathbf{x}',t')}{\partial t^2} - \nabla^2 p(\mathbf{x},t,\mathbf{x}',t') = s(\mathbf{x}',t') \tag{14}$$

Green's Function

If the source $s(\mathbf{x}',t')$ in equation (10) is a point source in space and an impulse in time, then the Green's function satisfies the acoustic wave equation for a constant isotropic medium $\forall \mathbf{x} \in V$, $\forall t \in \mathbb{R}$.

$$\frac{1}{c_0^2}\frac{\partial^2 g(\mathbf{x},t,\mathbf{x}',t')}{\partial t^2} - \nabla^2 g(\mathbf{x},t,\mathbf{x}',t') = \delta(\mathbf{x}-\mathbf{x}')\delta(t-t') \tag{15}$$

Spatial reciprocity lets us write

$$g(\mathbf{x},t,\mathbf{x}',t') = g(\mathbf{x}',t,\mathbf{x},t') \tag{16}$$

Also, since we have assumed that the model parameters are time invariant, we can shift the source in time and write

$$g(\mathbf{x},t,\mathbf{x}',t') = g(\mathbf{x},t-t',\mathbf{x}',0) \tag{17}$$

Analytical Solution to the Acoustic Wave Equation

The solution of equation (10) can be written $\forall \mathbf{x} \in V$, $\forall t \in \mathbb{R}$ as

$$p(\mathbf{x},t) = \int_{\mathbf{x}'\in V}\int_{t'\in-\infty}^{+\infty} g(\mathbf{x},t,\mathbf{x}',t')s(\mathbf{x}',t')\,dt'\,d\mathbf{x}' \tag{18}$$

By using this equation together with the time shifting property from equation (17) we get

$$p(\mathbf{x},t) = \int_{\mathbf{x}'\in V}\int_{t'\in-\infty}^{+\infty} g(\mathbf{x},t-t',\mathbf{x}',0)s(\mathbf{x}',t')\,dt'\,d\mathbf{x}' \tag{19}$$

We recognize the inner integral as temporal convolution

$$p(\mathbf{x},t) = \int_{\mathbf{x}'\in V} g(\mathbf{x},t,\mathbf{x}',0) * s(\mathbf{x}',t)\,d\mathbf{x}' \tag{20}$$

Finally, if the seismic source is a point source in space $\mathbf{x_s}$, and a signature in time $f(t)$, such that $s(\mathbf{x},t) = f(t)\delta(\mathbf{x}-\mathbf{x_s})$, then equation (20) simplifies to

$$p(\mathbf{x},t) = g(\mathbf{x},t,\mathbf{x_s},0) * f(t) \tag{21}$$

Reciprocity Theorems

Consider the region of interest, $V \subset \mathbb{R}^3$, which is a time-invariant domain in space. We denote the surface of V by $S \subset \mathbb{R}^2$ and let the normal vectors n_i on S be directed away from V. The reciprocity theorems are used to relate two non-identical acoustic states that occur in V (Fokkema and van den Berg, 1993). Here, we let the two states be the unperturbed and perturbed states described by equations (10) and (14), respectively. Furthermore, we

let the source in the unperturbed state be a point source in space and an impulse in time. Then, the Green's function satisfies the acoustic wave equation $\forall \mathbf{x} \in V$ and $\forall t \in \mathbb{R}$, and the two states can be expressed as follows.

Unperturbed state:

$$\frac{1}{c_0^2}\frac{\partial^2 g(\mathbf{x}, t, \mathbf{x}', t')}{\partial t^2} - \nabla^2 g(\mathbf{x}, t, \mathbf{x}', t') = \delta(\mathbf{x} - \mathbf{x}')\delta(t - t') \tag{22}$$

Perturbed state:

$$\frac{1 + \alpha(\mathbf{x})}{c_0^2}\frac{\partial^2 p(\mathbf{x}, t, \mathbf{x}', t')}{\partial t^2} - \nabla^2 p(\mathbf{x}, t, \mathbf{x}', t') = s(\mathbf{x}', t') \tag{23}$$

In order to derive the convolution type reciprocity theorem, we use Green's second identity. This identity is a special case of Gauss' theorem which relates the flow of a vector field across a surface to the behavior of the field inside the volume. Green's second identity takes the following form.

$$\int\limits_{\mathbf{x}' \in S} \Big[A(\mathbf{x}')\nabla B(\mathbf{x}') - B(\mathbf{x}')\nabla A(\mathbf{x}') \Big] n_i \, d\mathbf{x}' = \int\limits_{\mathbf{x}' \in V} \Big[A(\mathbf{x}')\nabla^2 B(\mathbf{x}') - B(\mathbf{x}')\nabla^2 A(\mathbf{x}') \Big] d\mathbf{x}' \tag{24}$$

where A and B are any scalar functions that are continuously differentiable on V. Then, we substitute A and B for $p(\mathbf{x}, t, \mathbf{x}', t')$ and $g(\mathbf{x}, t - t', \mathbf{x}', 0)$. Note that the Green's function is time-shifted according to (17).

$$\begin{aligned} &\int\limits_{\mathbf{x}' \in S} \Big[p(\mathbf{x}, t, \mathbf{x}', t')\nabla g(\mathbf{x}, t - t', \mathbf{x}', 0) - g(\mathbf{x}, t - t', \mathbf{x}', 0)\nabla p(\mathbf{x}, t, \mathbf{x}', t) \Big] n_i \, d\mathbf{x}' \\ &= \int\limits_{\mathbf{x}' \in V} \Big[p(\mathbf{x}, t, \mathbf{x}', t')\nabla^2 g(\mathbf{x}, t - t', \mathbf{x}', 0) - g(\mathbf{x}, t - t', \mathbf{x}', 0)\nabla^2 p(\mathbf{x}, t, \mathbf{x}', t) \Big] d\mathbf{x}' \end{aligned} \tag{25}$$

we integrate the terms over the time domain, $t' \in \mathbb{R}$.

$$\begin{aligned} &\int\limits_{t'=-\infty}^{+\infty} \int\limits_{\mathbf{x}' \in S} \Big[p(\mathbf{x}, t, \mathbf{x}', t')\nabla g(\mathbf{x}, t - t', \mathbf{x}', 0) - g(\mathbf{x}, t - t', \mathbf{x}', 0)\nabla p(\mathbf{x}, t, \mathbf{x}', t) \Big] n_i \, d\mathbf{x}' \, dt' \\ &= \int\limits_{t'=-\infty}^{+\infty} \int\limits_{\mathbf{x}' \in V} \Big[p(\mathbf{x}, t, \mathbf{x}', t')\nabla^2 g(\mathbf{x}, t - t', \mathbf{x}', 0) - g(\mathbf{x}, t - t', \mathbf{x}', 0)\nabla^2 p(\mathbf{x}, t, \mathbf{x}', t) \Big] d\mathbf{x}' \, dt' \end{aligned} \tag{26}$$

Then we can express the above equation using temporal convolution.

$$\int_{\mathbf{x}'\in S} \Big[p(\mathbf{x},t,\mathbf{x}') * \nabla g(\mathbf{x},t,\mathbf{x}') - g(\mathbf{x},t,\mathbf{x}') * \nabla p(\mathbf{x},t,\mathbf{x}')\Big] n_i \, d\mathbf{x}' \tag{27}$$
$$= \int_{\mathbf{x}'\in V} \Big[p(\mathbf{x},t,\mathbf{x}') * \nabla^2 g(\mathbf{x},t,\mathbf{x}') - g(\mathbf{x},t,\mathbf{x}') * \nabla^2 p(\mathbf{x},t,\mathbf{x}')\Big] d\mathbf{x}'$$

The right side of this equation can be rewritten by using the wave equations from (22) and (23) to substitute the Laplacian terms.

$$\int_{\mathbf{x}'\in S} \Big[p(\mathbf{x},t,\mathbf{x}') * \nabla g(\mathbf{x},t,\mathbf{x}') - g(\mathbf{x},t,\mathbf{x}') * \nabla p(\mathbf{x},t,\mathbf{x}')\Big] n_i \, d\mathbf{x}' \tag{28}$$
$$= \int_{\mathbf{x}'\in V} \Big[p(\mathbf{x},t,\mathbf{x}') * \Big(\frac{1}{c_0^2}\frac{\partial^2 g(\mathbf{x},t,\mathbf{x}')}{\partial t^2} - \delta(\mathbf{x}-\mathbf{x}')\delta(t)\Big)\Big] d\mathbf{x}'$$
$$- \int_{\mathbf{x}'\in V} \Big[g(\mathbf{x},t,\mathbf{x}') * \Big(\frac{1+\alpha(\mathbf{x})}{c_0^2}\frac{\partial^2 p(\mathbf{x},t,\mathbf{x}')}{\partial t^2} - s(\mathbf{x}',t)\Big)\Big] d\mathbf{x}'$$

We write out the brackets

$$\int_{\mathbf{x}'\in S} \Big[p(\mathbf{x},t,\mathbf{x}') * \nabla g(\mathbf{x},t,\mathbf{x}') - g(\mathbf{x},t,\mathbf{x}') * \nabla p(\mathbf{x},t,\mathbf{x}')\Big] n_i \, d\mathbf{x}' \tag{29}$$
$$= \int_{\mathbf{x}'\in V} \Big[\frac{p(\mathbf{x},t,\mathbf{x}')}{c_0^2} * \frac{\partial^2 g(\mathbf{x},t,\mathbf{x}')}{\partial t^2} - p(\mathbf{x},t,\mathbf{x}') * \delta(\mathbf{x}-\mathbf{x}')\delta(t)\Big] d\mathbf{x}'$$
$$- \int_{\mathbf{x}'\in V} \Big[g(\mathbf{x},t,\mathbf{x}') * \frac{1+\alpha(\mathbf{x})}{c_0^2}\frac{\partial^2 p(\mathbf{x},t,\mathbf{x}')}{\partial t^2} - g(\mathbf{x},t,\mathbf{x}') * s(\mathbf{x}',t)\Big] d\mathbf{x}'$$

The two terms $p(\mathbf{x},t,\mathbf{x}') * \frac{\partial^2 g(\mathbf{x},t,\mathbf{x}')}{\partial t^2}$ and $g(\mathbf{x},t,\mathbf{x}') * \frac{\partial^2 p(\mathbf{x},t,\mathbf{x}')}{\partial t^2}$ are the same (See Appendix A). After cancelling these terms, we have

$$\int_{\mathbf{x}'\in S} \Big[p(\mathbf{x},t,\mathbf{x}') * \nabla g(\mathbf{x},t,\mathbf{x}') - g(\mathbf{x},t,\mathbf{x}') * \nabla p(\mathbf{x},t,\mathbf{x}')\Big] n_i \, d\mathbf{x}' \tag{30}$$
$$= \int_{\mathbf{x}'\in V} \Big[g(\mathbf{x},t,\mathbf{x}') * s(\mathbf{x}',t)\Big] d\mathbf{x}' - \int_{\mathbf{x}'\in V} \Big[g(\mathbf{x},t,\mathbf{x}') * \frac{\alpha(\mathbf{x})}{c_0^2}\frac{\partial^2 p(\mathbf{x},t,\mathbf{x}')}{\partial t^2}\Big] d\mathbf{x}'$$
$$- \int_{\mathbf{x}'\in V} \Big[p(\mathbf{x},t,\mathbf{x}') * \delta(\mathbf{x}-\mathbf{x}')\delta(t)\Big] d\mathbf{x}'$$

We perform the integral in the last term, which yields $p(\mathbf{x}', t')$. Then we rearrange the equation as an expression for $p(\mathbf{x}', t')$.

$$
\begin{aligned}
p(\mathbf{x}', t') = & \int\limits_{\mathbf{x}' \in V} \Big[g(\mathbf{x}, t, \mathbf{x}') * s(\mathbf{x}', t) \Big] d\mathbf{x}' \\
& - \int\limits_{\mathbf{x}' \in V} \left[g(\mathbf{x}, t, \mathbf{x}') * \frac{\alpha(\mathbf{x})}{c_0^2} \frac{\partial^2 p(\mathbf{x}, t, \mathbf{x}')}{\partial t^2} \right] d\mathbf{x}' \\
& - \int\limits_{\mathbf{x}' \in S} \Big[p(\mathbf{x}, t, \mathbf{x}') * \nabla g(\mathbf{x}, t, \mathbf{x}') - g(\mathbf{x}, t, \mathbf{x}') * \nabla p(\mathbf{x}, t, \mathbf{x}') \Big] n_i \, d\mathbf{x}'
\end{aligned}
\tag{31}
$$

This is the convolution type reciprocity theorem which relates the solution of the acoustic wave equation in the unperturbed model, $g(\mathbf{x}, t, \mathbf{x}', t')$, to that of the perturbed model, $p(\mathbf{x}, t, \mathbf{x}', t')$. More specifically, it says that $\forall \mathbf{x}' \in V$ and $\forall t' \in \mathbb{R}$, the pressure in the perturbed model, $p(\mathbf{x}', t')$, can be expressed as a sum of contributions from the unperturbed model. The first term on the right side of equation (31) is the source contribution, the second term is the contribution from the model velocity perturbation, and the third term is the boundary condition contributions.

Reconstructing the Wavefield

With the reciprocity theorem established, we will now look at how it can be used to obtain the original source wavefield and the scattered wavefield (e.g. the first and second term on the right side of equation (31)), given $p(\mathbf{x}', t')$. To better visualize the concept, we consider a 2D experiment.

Let $V \in \mathbb{R}^2$ be a semi-infinite set and our model of interest. Furthermore, let $S \in \mathbb{R}$ be the line enclosing V. We define two subsurface models in V, shown in Figure 1. Both models have constant mass density and they are constrained above by a free surface. 1a has a velocity perturbation in form of a sedimentary package underlying a column of water. 1b is a water column with no velocity perturbation. The behavior of an acoustic wave propagating in these models is described by equation (23) for the perturbed model, and by equation (22) for the unperturbed model.

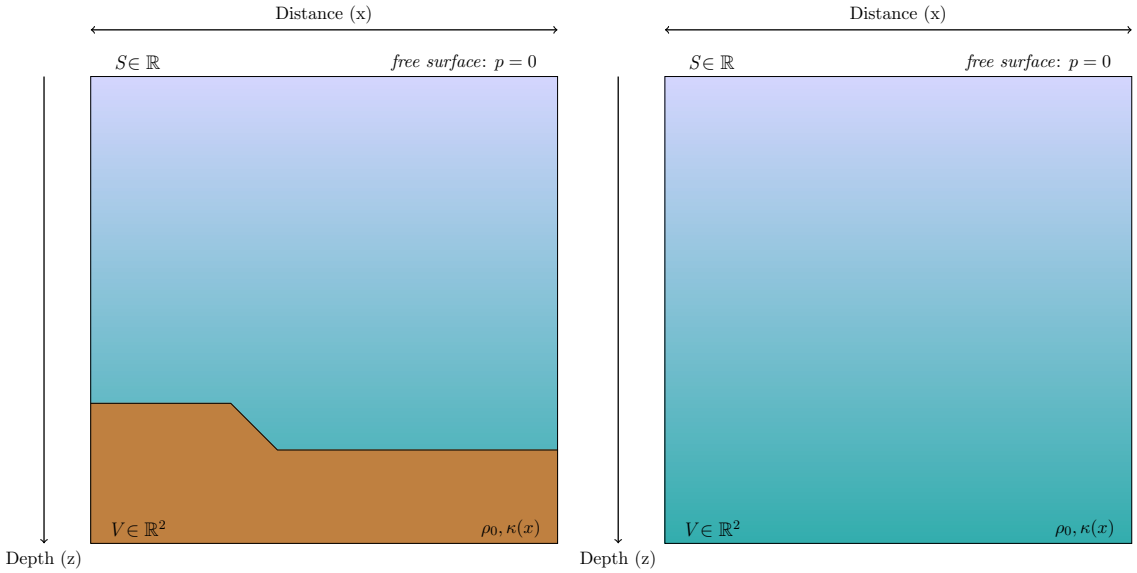

Figure 1: Schematic view of an (a) perturbed and (b) unperturbed velocity model. The brown layer in (a) represents the velocity pertubation, which can be any layer configuration in the subsurface.

We set up a simple seismic experiment using these two models. The experiment has two parts. In the first part, we generate multicomponent seismic data using the pertubed model. In the second part, we inject the recorded data into the unperturbed model. For the first part, consider a point source that is situated in the water column at $(x, z) = (x_s, z_s)$. The source fires a single shot and the resulting wavefield is recorded along a receiver array that is situated below the source at $z = z_r$. The data is recorded as multicomponent data, where both the pressure field and the velocity field are recorded.

In the second part, the recorded multicomponent data is injected along an injector array in the unperturbed model at $z = z_r$. There are two receiver arrays that record the resulting wavefields, one above the injector at $z = z_u$ and one below the injector at $z = z_l$. The setup for the experiment is shown in Figure 2. The multicomponent data is injected into the unperturbed model by imposing the data as boundary conditions. That is, we divide the volume of interest into two subvolumes $(V_1, V_2) \subset V$ that are enclosed by surfaces (S_1, S_2) and separated at the injector array, as Figure 3 shows. By injecting the data into the subvolumes in the unperturbed model, it is possible to obtain the original source wavefield and the scattered wavefield separately, as we show in the following two sections. We will use subscript a to denote quantities in the perturbed model, and subscripts b for quantities in the unperturbed model.

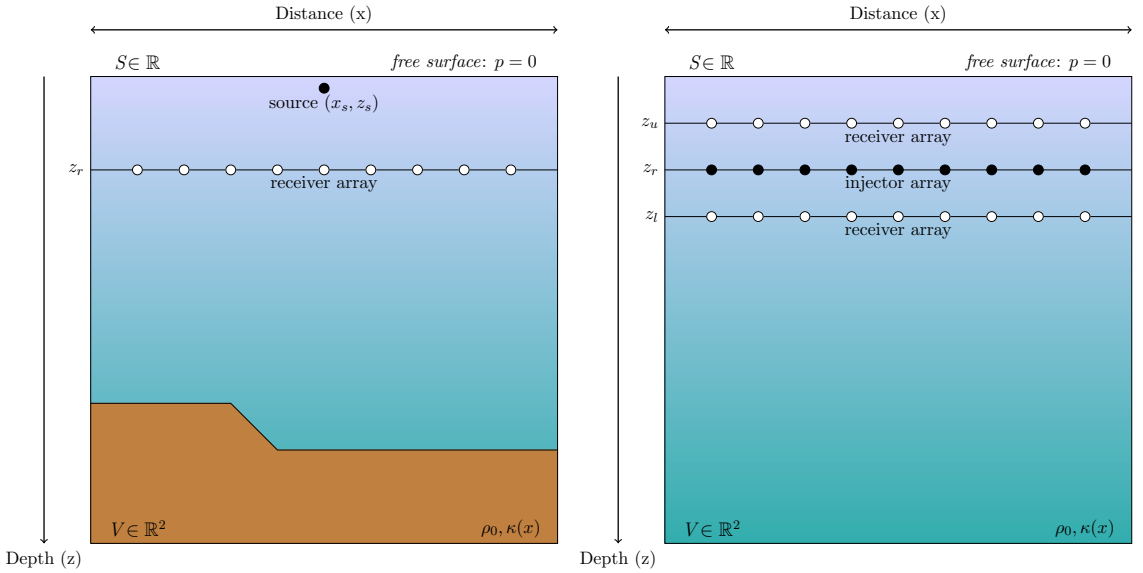

Figure 2: Schematic view of the setup for the seismic experiment. A point source is fired in (a) and the resulting wavefield is recorded along the receiver array at $z = z_r$ as multi-component data. Then, this data is injected into (b) along the injector array. The injected wavefields are then recorded at receiver arrays above and below the injector.

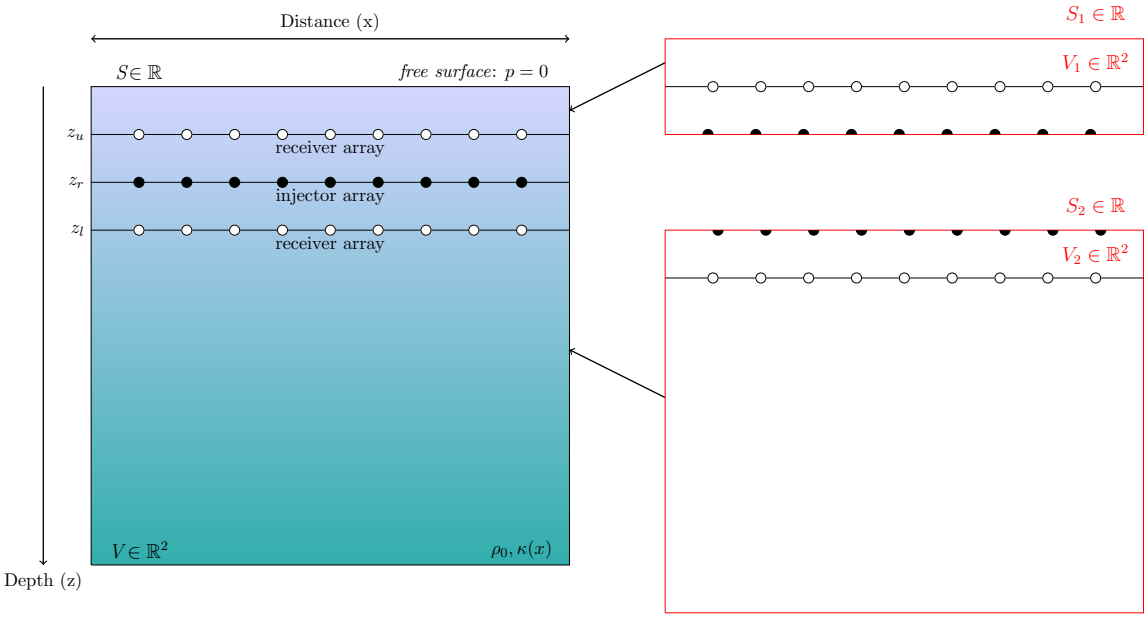

Figure 3: The data is injected into the unperturrbed model by imposing the data as boundary conditions. Therefore, we split the model at the injector array into $(V_1, V_2) \subset V$ and consider the two subvolumes separately.

The Scattered Wavefield

The scattered wavefield is the wavefield created by the velocity perturbation in the perturbed model. This wavefield is obtained by injecting the recorded data into V_1 and recording the data above the injector array. To show this, we consider the implications of the divergence theorem on V_1 in the perturbed and unperturbed model. Figure 4 shows V_1 of (a) the perturbed, and (b) the unperturbed model.

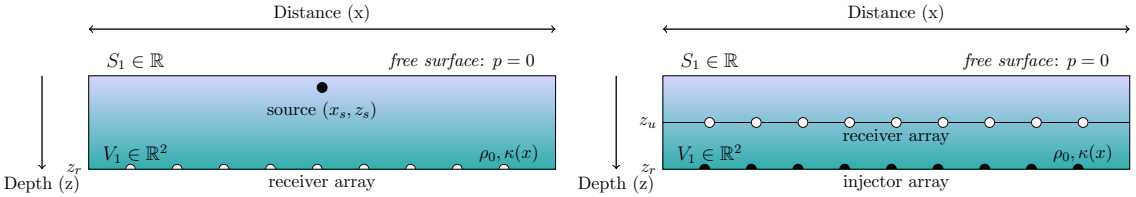

Figure 4: Schematic view of submodels $V_1 \subset V$ for (a) the perturbed model and (b) the unperturbed model.

For V_1 in the perturbed model, we have a source, but no velocity perturbations. This means that $\alpha(\mathbf{x}) = 0$, and the reciprocity theorem from equation (31) can therefore be written as follows for this subvolume.

$$\begin{aligned} p_a(\mathbf{x}', t') = &\int\limits_{\mathbf{x}' \in V_1} \Big[g(\mathbf{x}, t, \mathbf{x}') * s(\mathbf{x}', t) \Big] d\mathbf{x}' \\ &- \int\limits_{\mathbf{x}' \in S_1} \Big[p(\mathbf{x}, t, \mathbf{x}') * \nabla g(\mathbf{x}, t, \mathbf{x}') - g(\mathbf{x}, t, \mathbf{x}') * \nabla p(\mathbf{x}, t, \mathbf{x}') \Big] n_i \, d\mathbf{x}' \end{aligned} \tag{32}$$

where $p_a(\mathbf{x}', t')$ is the pressure at any point in V_1. For V_1 in the unperturbed model there is no source nor velocity pertubation, such that the reciporcity theorem can be written

$$p_b(\mathbf{x}', t') = - \int\limits_{\mathbf{x}' \in S_1} \Big[p(\mathbf{x}, t, \mathbf{x}') * \nabla g(\mathbf{x}, t, \mathbf{x}') - g(\mathbf{x}, t, \mathbf{x}') * \nabla p(\mathbf{x}, t, \mathbf{x}') \Big] n_i \, d\mathbf{x}' \tag{33}$$

Firing a point source in V_1 of the perturbed model and recording it along the boundary gives the same wavefield as injecting the source along the boundary into V_1 of the unperturbed model. Therefore, we can substitute (32) in on the right side of (33) and write

$$\begin{aligned} p_b(\mathbf{x}', t') = &- \int\limits_{\mathbf{x}' \in V_1} \Big[g(\mathbf{x}, t, \mathbf{x}') * s(\mathbf{x}', t) \Big] d\mathbf{x}' \\ &+ \int\limits_{\mathbf{x}' \in S_1} \Big[p(\mathbf{x}, t, \mathbf{x}') * \nabla g(\mathbf{x}, t, \mathbf{x}') - g(\mathbf{x}, t, \mathbf{x}') * \nabla p(\mathbf{x}, t, \mathbf{x}') \Big] n_i \, d\mathbf{x}' \end{aligned} \tag{34}$$

where the signs on the right side of the equation are reversed because we are injecting in the direction opposite to n_i. The contribution across the boundaries is equal to the data recorded from the entire volume of the perturbed model. That is,

$$p_b(\mathbf{x}', t') = -\int\limits_{\mathbf{x}' \in V_1} \Big[g(\mathbf{x}, t, \mathbf{x}') * s(\mathbf{x}', t) \Big] d\mathbf{x}' \tag{35}$$

$$+p(\mathbf{x}', t') \tag{36}$$

We use equation (31) to substitute for $p(\mathbf{x}', t')$

$$\begin{aligned} p_b(\mathbf{x}', t') = &-\int\limits_{\mathbf{x}' \in V_1} \Big[g(\mathbf{x}, t, \mathbf{x}') * s(\mathbf{x}', t) \Big] d\mathbf{x}' \\ &+\Bigg(\int\limits_{\mathbf{x}' \in V} \Big[g(\mathbf{x}, t, \mathbf{x}') * s(\mathbf{x}', t) \Big] d\mathbf{x}' \\ &- \int\limits_{\mathbf{x}' \in V} \left[g(\mathbf{x}, t, \mathbf{x}') * \frac{\alpha(\mathbf{x})}{c_0^2} \frac{\partial^2 p(\mathbf{x}, t, \mathbf{x}')}{\partial t^2} \right] d\mathbf{x}' \\ &- \int\limits_{\mathbf{x}' \in S} \Big[p(\mathbf{x}, t, \mathbf{x}') * \nabla g(\mathbf{x}, t, \mathbf{x}') - g(\mathbf{x}, t, \mathbf{x}') * \nabla p(\mathbf{x}, t, \mathbf{x}') \Big] n_i \, d\mathbf{x}' \Bigg) \end{aligned} \tag{37}$$

the two first terms cancel, and since the model volume V is a semi infinite region bounded above by a free surface, we assume that there are no contributions along the model surface. That is, we assume that the pressure p and the Green's function g are zero at the free surface. Then we are left with

$$p_b(\mathbf{x}', t') = -\int\limits_{\mathbf{x}' \in V} \left[g(\mathbf{x}, t, \mathbf{x}') * \frac{\alpha(\mathbf{x})}{c_0^2} \frac{\partial^2 p(\mathbf{x}, t, \mathbf{x}')}{\partial t^2} \right] d\mathbf{x}' \tag{38}$$

This result says that the wavefield recorded above the datainjector in the unperturbed model equals the wavefield contributed by the velocity model perturbation with reversed polarity. That is, the source wavefield has no contribution here.

The Source Wavefield

The source wavefield is our quantity of interest, and it is obtained in a similar fashion as the scattered wavefield. The recorded seismic data is injected into the subvolume V_2 of the unperturbed model. Consider Figure 5 of V_2 , where (a) is the perturbed model, and (b) is the unperturbed model.

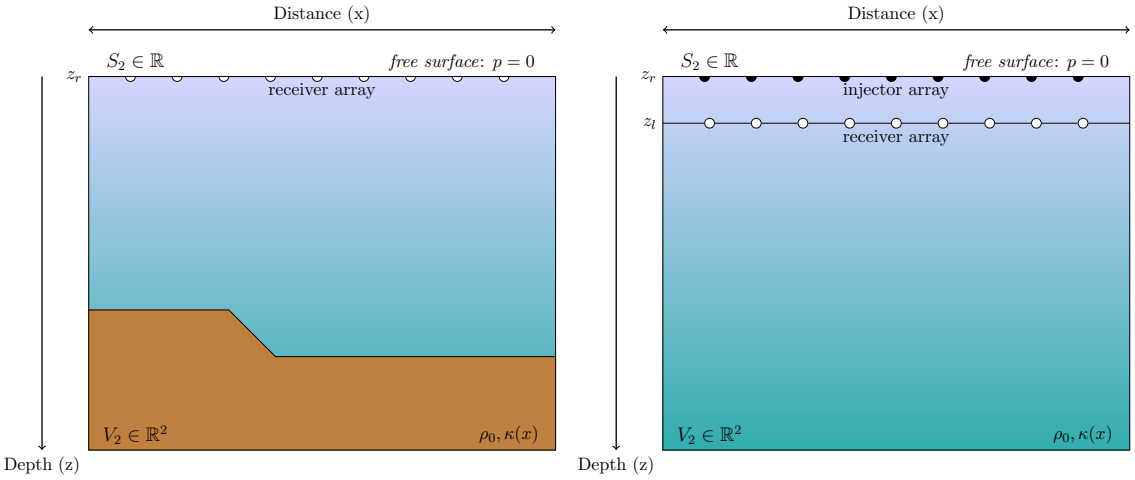

Figure 5: Schematic view of submodels $V_2 \subset V$ for (a) the perturbed model and (b) the unperturbed model.

In (a) there is no source, but there is a velocity perturbation and communication along the upper boundary. Therefore, the reciprocity theorem for this subvolume can be written as

$$p_a(\mathbf{x}', t') = -\int_{\mathbf{x}' \in V_2} \left[g(\mathbf{x}, t, \mathbf{x}') * \frac{\alpha(\mathbf{x})}{c_0^2} \frac{\partial^2 p(\mathbf{x}, t, \mathbf{x}')}{\partial t^2} \right] d\mathbf{x}' \tag{39}$$
$$- \int_{\mathbf{x}' \in S_2} \Big[p(\mathbf{x}, t, \mathbf{x}') * \nabla g(\mathbf{x}, t, \mathbf{x}') - g(\mathbf{x}, t, \mathbf{x}') * \nabla p(\mathbf{x}, t, \mathbf{x}') \Big] n_i \, d\mathbf{x}'$$

where $p_a(\mathbf{x}', t')$ is the pressure at any point in V_2. The reciprocity theorem for V_2 in the unperturbed model takes the same form as in equation (33).

$$p_b(\mathbf{x}', t') = -\int_{\mathbf{x}' \in S_2} \Big[p(\mathbf{x}, t, \mathbf{x}') * \nabla g(\mathbf{x}, t, \mathbf{x}') - g(\mathbf{x}, t, \mathbf{x}') * \nabla p(\mathbf{x}, t, \mathbf{x}') \Big] n_i \, d\mathbf{x}' \tag{40}$$

Recording the scattered wavefield along the boundary in the perturbed model is the same as injecting the scattered wavefield into V_2 of the unperturbed model. We therefore substitute (39) in on the right side of (40) and write

$$p_b(\mathbf{x}', t') = \int_{\mathbf{x}' \in V_2} \left[g(\mathbf{x}, t, \mathbf{x}') * \frac{\alpha(\mathbf{x})}{c_0^2} \frac{\partial^2 p(\mathbf{x}, t, \mathbf{x}')}{\partial t^2} \right] d\mathbf{x}' \tag{41}$$
$$+ \int_{\mathbf{x}' \in S_2} \Big[p(\mathbf{x}, t, \mathbf{x}') * \nabla g(\mathbf{x}, t, \mathbf{x}') - g(\mathbf{x}, t, \mathbf{x}') * \nabla p(\mathbf{x}, t, \mathbf{x}') \Big] n_i \, d\mathbf{x}'$$

Again, the signs are reversed because we inject in the direction oposite to n_i. The contributions across the boundary are equal to the data recorded in the entire perturbed model, which allows us to write

$$p_b(\mathbf{x}', t') = \int\limits_{\mathbf{x}' \in V_2} \left[g(\mathbf{x}, t, \mathbf{x}') * \frac{\alpha(\mathbf{x})}{c_0^2} \frac{\partial^2 p(\mathbf{x}, t, \mathbf{x}')}{\partial t^2} \right] d\mathbf{x}' + p(\mathbf{x}', t') \tag{42}$$

Then we substitute for $p(\mathbf{x}', t')$ using equation (31).

$$\begin{aligned} p_b(\mathbf{x}', t') = & \int\limits_{\mathbf{x}' \in V_2} \left[g(\mathbf{x}, t, \mathbf{x}') * \frac{\alpha(\mathbf{x})}{c_0^2} \frac{\partial^2 p(\mathbf{x}, t, \mathbf{x}')}{\partial t^2} \right] d\mathbf{x}' \\ & + \Bigg(\int\limits_{\mathbf{x}' \in V} \left[g(\mathbf{x}, t, \mathbf{x}') * s(\mathbf{x}', t) \right] d\mathbf{x}' \\ & - \int\limits_{\mathbf{x}' \in V} \left[g(\mathbf{x}, t, \mathbf{x}') * \frac{\alpha(\mathbf{x})}{c_0^2} \frac{\partial^2 p(\mathbf{x}, t, \mathbf{x}')}{\partial t^2} \right] d\mathbf{x}' \\ & - \int\limits_{\mathbf{x}' \in S} \left[p(\mathbf{x}, t, \mathbf{x}') * \nabla g(\mathbf{x}, t, \mathbf{x}') - g(\mathbf{x}, t, \mathbf{x}') * \nabla p(\mathbf{x}, t, \mathbf{x}') \right] n_i \, d\mathbf{x}' \Bigg) \end{aligned} \tag{43}$$

Here, two terms cancel and since we have a semi infinite region bounded above by the free surface we assume there to be no contributions along the surface. This leaves us with

$$p_b(\mathbf{x}', t') = \int\limits_{\mathbf{x}' \in V} \left[g(\mathbf{x}, t, \mathbf{x}') * s(\mathbf{x}', t) \right] d\mathbf{x}' \tag{44}$$

This result says that by injecting the data into V_2 in the unperturbed model and recording below the injector, we retrieve the source wavefield. That is, there is no contributions from the model perturbation here. This is the same result that Weglein and Secrest (1990) obtained for the frequency-space domain, and it is the result that we want to exploit for full waveform inversion.

Injector Representation

The injector that is used for injecting the multicomponent data $p(\mathbf{x}', t')$ is a combination of a monopole and a dipole. The expression for the injector is derived from equation (33). We split the equation into two integrals which we evaluate separately.

$$p(\mathbf{x}', t') = \int\limits_{\mathbf{x}' \in S} \left[g(\mathbf{x}, t, \mathbf{x}') * \nabla p(\mathbf{x}, t, \mathbf{x}') \right] n_i \, d\mathbf{x}' - \int\limits_{\mathbf{x}' \in S} \left[p(\mathbf{x}, t, \mathbf{x}') * \nabla g(\mathbf{x}, t, \mathbf{x}') \right] n_i \, d\mathbf{x}' \tag{45}$$

First we consider the first integral in equation (45).

$$\int\limits_{\mathbf{x}'\in S} \Big[g(\mathbf{x},t,\mathbf{x}') * \nabla p(\mathbf{x},t,\mathbf{x}') \Big] n_i \, d\mathbf{x}' \tag{46}$$

By using a property of the Dirac delta function, it is possible to write

$$g(\mathbf{x},t,\mathbf{x}') = \int\limits_{\mathbf{x}''\in V} g(\mathbf{x}'',t,\mathbf{x}')\delta(\mathbf{x}''-\mathbf{x})d\mathbf{x}'' \tag{47}$$

If we insert this into equation (46) we get

$$\int\limits_{\mathbf{x}'\in S} \Big[\Big(\int\limits_{\mathbf{x}''\in V} g(\mathbf{x}'',t,\mathbf{x}')\delta(\mathbf{x}''-\mathbf{x})d\mathbf{x}'' \Big) * \nabla p(\mathbf{x},t,\mathbf{x}') \Big] n_i \, d\mathbf{x}' \tag{48}$$

which we can rewrite as

$$\int\limits_{\mathbf{x}''\in V} g(\mathbf{x}'',t,\mathbf{x}') * s^{(m)} d\mathbf{x}'' \tag{49}$$

where $s^{(m)} = \int\limits_{\mathbf{x}'\in S} \Big[\nabla p(\mathbf{x},t,\mathbf{x}')\delta(\mathbf{x}''-\mathbf{x}) \Big] n_i \, d\mathbf{x}'$, is a monopole source. The second term of the integral equation in (45) is

$$-\int\limits_{\mathbf{x}'\in S} \Big[p(\mathbf{x},t,\mathbf{x}') * \nabla g(\mathbf{x},t,\mathbf{x}') \Big] n_i \, d\mathbf{x}' \tag{50}$$

Also here we use a property of the Dirac delta function. In general we can write for a differentiable function f

$$\nabla f(\mathbf{x}) = -\int\limits_{\mathbf{x}''\in V} f(\mathbf{x}'')\nabla\delta(\mathbf{x}''-\mathbf{x})d\mathbf{x}'' \tag{51}$$

Using this relation with $f(\mathbf{x}) = g(\mathbf{x},t,\mathbf{x}')$ gives

$$\nabla g(\mathbf{x},t,\mathbf{x}') = -\int\limits_{\mathbf{x}''\in V} g(\mathbf{x}'',t,\mathbf{x}')\nabla\delta(\mathbf{x}''-\mathbf{x})d\mathbf{x}'' \tag{52}$$

We insert this back into equation (50) to get

$$\int\limits_{\mathbf{x}'\in S} \Big[p(\mathbf{x},t,\mathbf{x}') * \Big(\int\limits_{\mathbf{x}''\in V} g(\mathbf{x}'',t,\mathbf{x}')\nabla\delta(\mathbf{x}''-\mathbf{x})d\mathbf{x}'' \Big) \Big] n_i \, d\mathbf{x}' \tag{53}$$

We then rewrite this equation as follows

$$\int_{\mathbf{x}''\in V} g(\mathbf{x}'', t, \mathbf{x}') * s^{(d)} d\mathbf{x}'' \tag{54}$$

where $s^{(d)} = \int_{\mathbf{x}'\in S} \Big[p(\mathbf{x}, t, \mathbf{x}')\nabla\delta(\mathbf{x}''-\mathbf{x})\Big] n_i \, d\mathbf{x}'$, is a dipole. By collecting the rewritten terms in equations (49) and (54) we can write equation (45) as

$$\int_{\mathbf{x}''\in V} g(\mathbf{x}'', t, \mathbf{x}') * s(\mathbf{x}, t, \mathbf{x}', \mathbf{x}'') d\mathbf{x}'' \tag{55}$$

where $s(\mathbf{x}, t, \mathbf{x}', \mathbf{x}'') = s^{(m)} + s^{(d)}$, and $s^{(m)}$ and $s^{(d)}$ are on the following form.

$$s^{(m)} = \int_{\mathbf{x}'\in S} \Big[\nabla p(\mathbf{x}, t, \mathbf{x}')\delta(\mathbf{x}'' - \mathbf{x})\Big] n_i \, d\mathbf{x}' \tag{56}$$

$$s^{(d)} = \int_{\mathbf{x}'\in S} \Big[p(\mathbf{x}, t, \mathbf{x}')\nabla\delta(\mathbf{x}'' - \mathbf{x})\Big] n_i \, d\mathbf{x}' \tag{57}$$

SOLVING THE ACOUSTIC WAVE EQUATION

In order to test the concepts derived in the previous section, we created grid-based models of the subsurface and used finite difference methods to discretize and solve the equations.

Finite Difference

The acoustic wave equation is a differential equation, and its solution has to be such that the derivatives of the solution satisfy a certain relationship on a given domain in time and/or space. The solution must also satisfy a set of boundary conditions along the edges of the given domain. All these requirements make it difficult to solve the acoustic wave equation, and a theoretical solution to the problem can often be unobtainable (Leveque, 2007). If one can accept a certain degree of error in the solution, it is convenient to use methods for approximating the solution. One such method for approximationg solutions to differential equations is the finite difference (FD) method.

The method works by approximating the derivatives of the differential equation such that the problem is reduced to a finite system of algebraic equations that can be solved instead of solving the differential equation (Leveque, 2007). A benefit of doing this is that a system of algebraic equations can be solved by a computer, which allows for large problem sizes. The essence of FD approximations can be understood by investigating the standard definition of the derivative. Let $f(x)$ be a function whose derivative exists $\forall x \in \mathbb{R}$. Then, the derivative of f can be defined as

$$f'(x) = \lim_{dx \to 0} \frac{f(x + dx) - f(x)}{dx} \tag{58}$$

By neglecting the limit and allowing the step size to be finite, $dx = \Delta x$, the equation can be written as

$$f'(x) \approx \frac{f(x + \Delta x) - f(x)}{\Delta x} \tag{59}$$

This equation gives an approximate relation between the function and its derivative. Equation (59) is known as the simple forward finite difference operator and it states that the derivative of a smooth function f is approximately equal to the slope of the line interpolation between $f(x)$ and $f(x + \Delta x)$ (Leveque, 2007). Since the step size is finite, there is an error in the scheme. The simple forward operator is a first order method because the error in the scheme is proportional to Δx. In general, for an n-th order finite difference operator, the error is proportional to $(\Delta x)^n$.

The simple forward operator is a coarse approximation that converges slowly. The accuracy can be improved by using operators with additional function evaluations. One such operator is the central difference operator.

$$f'(x) \approx \frac{f(x + \Delta x) - f(x - \Delta x)}{2\Delta x} \tag{60}$$

This operator is of second order, which means that the error in the scheme is proportional to $(\Delta x)^2$. The simple forward operator and the central operator are both approximations of the first derivative of f. The FD method can also be used to approximate higher order derivatives. As an example, here is the simplest FD operator for a second order derivative f''.

$$f''(x) \approx \frac{f(x + \Delta x) - 2f(x) + f(x - \Delta x)}{(\Delta x)^2} \tag{61}$$

For a multivariate differential equation, such as the acoustic wave equation in (9), we can use different FD operators to approximate the derivative for each variable.

Solving the Acoustic Wave Equation

For the implementations in this work, we consider the acoustic wave equation with two spatial dimensions, where $\mathbf{x} = (x, z)$. Here, x is the offset dimension and z is the depth dimension. With two spatial dimensions, Newton's second law from equation (7) must be written for each dimension.

$$\rho_0 \ddot{u}_x(\mathbf{x}, t) = \nabla_x p(\mathbf{x}, t) \tag{62}$$

$$\rho_0 \ddot{u}_z(\mathbf{x}, t) = \nabla_z p(\mathbf{x}, t) \tag{63}$$

where we have used the dot notation ($\ddot{}$) to denote the second order temporal derivative. We don't specify the source coordinates or initiation time, and therefore we drop the $\mathbf{x}'$ and t' terms. Hooke's law for two spatial dimensions becomes

$$p(\mathbf{x},t) = \kappa(\mathbf{x})\Big[\nabla_x u_x(\mathbf{x},t) + \nabla_z u_z(\mathbf{x},t)\Big] + I(\mathbf{x},t) \tag{64}$$

Taking the second order temporal derivate of this equation gives us

$$\ddot{p}(\mathbf{x},t) = \kappa(\mathbf{x})\Big[\nabla_x \ddot{u}_x(\mathbf{x},t) + \nabla_z \ddot{u}_z(\mathbf{x},t)\Big] + \ddot{I}(\mathbf{x},t) \tag{65}$$

Discretizing in time and space

We discretize equations (62)-(65) for the two spatial dimensions $\mathbf{x} = (x, z)$ and the temporal dimension t as follows.

$$\begin{aligned} x_i &= (i-1)\Delta i, \quad i \in \{1, N_x\} \\ z_j &= (j-1)\Delta j, \quad j \in \{1, N_z\} \\ t_n &= (n-1)\Delta t, \quad n \in \{1, N_t\} \end{aligned} \tag{66}$$

where N_x and N_z are the number og discrete points in the spatial dimensions, and N_t is the number of discrete points in the temporal dimension. Δt, Δx, and Δz are the step sizes in each dimension. Furthermore, we want to use a compact notation:

$$\begin{aligned} p^n_{i,j} &= p(x_i = (i-1)\Delta i, z_j = (j-1)\Delta j, t_n = (n-1)\Delta t) \\ u^n_{i,j} &= u(x_i = (i-1)\Delta i, z_j = (j-1)\Delta j, t_n = (n-1)\Delta t) \end{aligned} \tag{67}$$

Then we can express Newton's second law from equations (62)-(63) as

$$\rho_0 \ddot{u}^n_{x_{i,j}} = \nabla_x \, p^n_{i,j} \tag{68}$$

$$\rho_0 \ddot{u}^n_{z_{i,j}} = \nabla_x \, p^n_{i,j} \tag{69}$$

and Hooke's law from equation (64) becomes

$$p^n_{i,j} = \kappa_j \Big[\nabla_x \, u^n_{x_{i,j}} + \nabla_z \, u^n_{z_{i,j}}\Big] + I_{i,j} \tag{70}$$

Note that the bulk modulus κ only has an index j, which means that it is constant in the offset dimension. Finally, the second order temporal derivative from equation (65) is

$$\ddot{p}^n_{i,j} = \kappa_j \Big[\nabla_x \, \ddot{u}^n_{x_{i,j}} + \nabla_z \, \ddot{u}^n_{z_{i,j}}\Big] + s_{i,j} \tag{71}$$

Solving the Acoustic Wave Equation on the Staggered Grid

To solve the discrete acoustic wave equation with two spatial dimensions, we use FD operators to find explicit expressions for the pressure p and particle acceleration $\ddot{u}$.This method is iterative and it advances in time using information from previous and current timesteps. We also make use of a concept called grid staggering (Virieux, 1986). This is a matematical manipulation with FD methods that improves the spatial accuracy of the discrete solution.

Consider equation (71). The second order temporal derivative on the left side of this equation can be approximated using the FD operator from equation (61).

$$\ddot{p}_{i,j}^{n} \approx \frac{p_{i,j}^{n+1} - 2p_{i,j}^{n} + p_{i,j}^{n-1}}{(\Delta t)^2} \tag{72}$$

By substituting this expression for the left side of equation (71) and rearranging the resulting expression, we get

$$\ddot{p}_{i,j}^{n+1} = 2p_{i,j}^{n} - p_{i,j}^{n-1} + (\Delta t)^2 \left[\nabla_x \ddot{u}_{x_{i,j}}^{n} + \nabla_z \ddot{u}_{z_{i,j}}^{n} \right] + s_{i,j}^{n} \tag{73}$$

This expression makes it possible to calculate the pressure at time $t = t_n + \Delta t$ if the pressure at the current time (t_n) and the previous time ($t_n - \Delta t$) are known, in addition to the current source value ($\ddot{I}$) and the the partial derivatives of the particle displacement (u_x and u_z). Similarly, we find an expression for the particle acceleration by considering equations (68) and (69). Here we introduce spatial grid staggering, where we evaluate the particle acceleration on grids that are shifted by half a grid point in space (Virieux, 1986). The purpose of doing this is that it allows us to use the central difference FD operator from equation (60) instead of the simple forward operator. This gives us a more accurate operator that converges more quickly. The concept of grid staggering is illustrated in Figure 6.

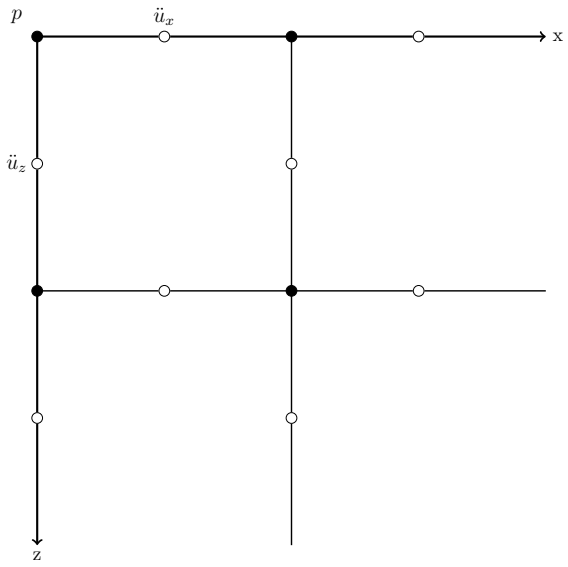

Figure 6: Schematic view of the staggered grid. The particle acceleration is shifted by half a grid point compared to the pressure.

To derive the explicit expression for the particle acceleration, we start with equations (68)-(69) and divide both sides of the equations by ρ_0.

$$\ddot{u}^n_{x_{i,j}} = \frac{1}{\rho_0}\nabla_x \, p^n_{i,j} \tag{74}$$

$$\ddot{u}^n_{z_{i,j}} = \frac{1}{\rho_0}\nabla_z \, p^n_{i,j} \tag{75}$$

Then we change the evaluation point to the staggered grid, by shifting the evaluation of (74) to $i = i + 1/2$ and the evaluation of (75) to $j = j + 1/2$.

$$\ddot{u}^n_{x_{i+1/2,j}} = \frac{1}{\rho_0}\nabla_x \, p^n_{i+1/2,j} \tag{76}$$

$$\ddot{u}^n_{z_{i,j+1/2}} = \frac{1}{\rho_0}\nabla_z \, p^n_{i,j+1/2} \tag{77}$$

We approximate the spatial derivative on the right side of the equations using the central operator from equation (60).

$$p^n_{x_{i+1/2,j}} = \frac{1}{\rho_0}\left[\frac{p^n_{x_{i+1,j}} - p^n_{x_{i,j}}}{\Delta x}\right] \tag{78}$$

$$p^n_{z_{i,j+1/2}} = \frac{1}{\rho_0}\left[\frac{p^n_{z_{i,j+1}} - p^n_{x_{i,j}}}{\Delta z}\right] \tag{79}$$

Because of the grid staggering, the spatial derivatives in equation (73) are now evaluated at the staggered grid

$$\ddot{p}^{n+1}_{i,j} = 2p^{n}_{i,j} - p^{n-1}_{i,j} + (\Delta t)^2 \Big[\nabla_x \ddot{u}^{n}_{x_{i+1/2,j}} + \nabla_z \ddot{u}^{n}_{z_{i,j+1/2}} \Big] + s^{n}_{i,j} \tag{80}$$

In order to shift the staggered grid back to the original grid, we replace the spatial derivatives in this equation with central difference operators and substitute in equations (76) and (77). The acoustic wave equation with two spatial dimensions can then be solved using equations (78) and (79) together with equation (80).

Adding the Source Term

In order to implement the data injector in equation (55) we must discretize the equation and use a discrete approximation of the Dirac delta function. The Dirac delta function is easy to work with in theory, but it is more difficult to implement in a practical model (Walden, 1999). The approximation we used to implement this function in a model with two spatial dimensions was $\delta(x, z) \approx 1/(\Delta x \Delta z)$. Furthermore, we used the central FD operator in equation (60) to approximate the spatial derivative of the Dirac delta function. Using the same discretization as in equation (66), we discretize the injector equation as follows.

$$\int\limits_{\mathbf{x}'' \in V} g(\mathbf{x}'', t, \mathbf{x}') * s(\mathbf{x}, t, \mathbf{x}', \mathbf{x}'') d\mathbf{x}'' = \sum_{n'=1}^{N_t} \sum_{i''=1, j''=1}^{V} g_{i'',j''}\, s^{n'}_{i'',j''}\, \Delta x'' \Delta z'' \Delta t' \tag{81}$$

For the monopole and dipole terms the discretizations become:

$$\begin{aligned} s^{(m)} &= \int\limits_{\mathbf{x}' \in S} \Big[\nabla p(\mathbf{x}, t, \mathbf{x}') \delta(\mathbf{x}'' - \mathbf{x}) \Big] n_i \, d\mathbf{x}' \qquad (82) \\ &= \sum_{i'=1}^{S} \nabla p_{i'} \delta \, \Delta x' + \sum_{j'=1}^{S} \nabla p_{j'} \delta \, \Delta z' \\ s^{(d)} &= \int\limits_{\mathbf{x}' \in S} \Big[p(\mathbf{x}, t, \mathbf{x}') \nabla \delta(\mathbf{x}'' - \mathbf{x}) \Big] n_i \, d\mathbf{x}' \qquad (83) \\ &= \sum_{i'=1}^{S} p_{i'} \frac{\delta_{i'+1} - \delta_{i'-1}}{2\Delta x} \Delta x' + \sum_{j'=1}^{S} p_{j'} \frac{\delta_{j'+1} - \delta_{j'-1}}{2\Delta z} \Delta z' \end{aligned}$$

where we replace the delta function with $1/(\Delta x \Delta z)$ at $(i'' = i, j'' = j)$. The central difference operator that is used to approximate $\nabla \delta(\mathbf{x}'' - \mathbf{x})$ could also be replaced by more accurate operators. The disadvantage of using a more accurate FD opearator is that it requires more function evaluations, which means that the dipole will span more grid points in the model.

NUMERICAL EXPERIMENT

We used the numerical implementations from the previous section to model the seismic experiment from Figure 2. We created two gridbased velocity models that resemble the conceptual models in Figure 1. They were both semi-infinite models with free surfaces above. The two models are shown in Figure 7, where (a) is the perturbed model, and (b) is the unperturbed model.

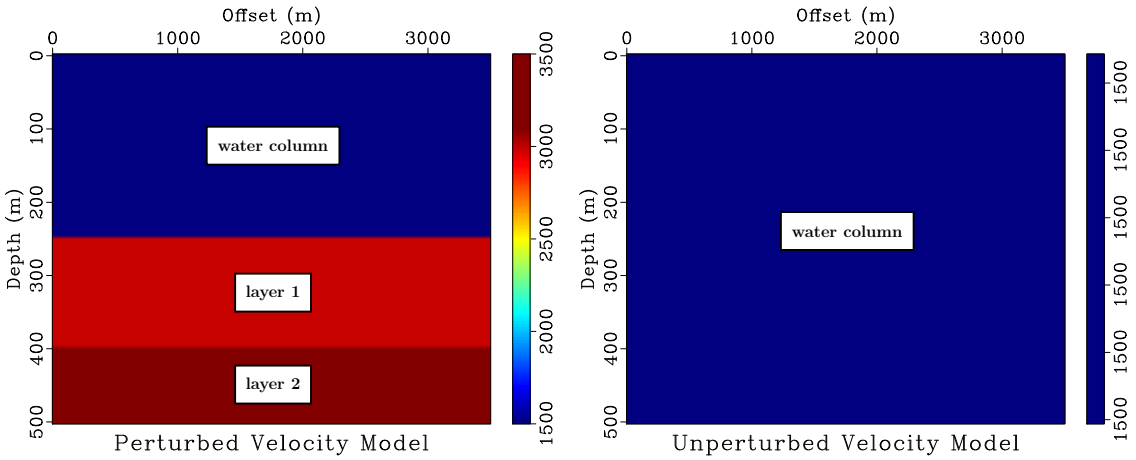

Figure 7: Subsurface velocity models used for the numerical experiment.

The perturbed velocity model has two perfectly flat layers underlying a column of water, and the unperturbed model is a single column of water. Using these models, we set up the seismic experiment from Figure 2. That is, we initiated a point source in the perturbed model and recorded multicomponent data along a receiver array. Then, the data was injected into the unperturbed model and recorded at receivers above and below the injector. The source pulse was created using a Ricker pulse with a peak frequency of $15Hz$, and a timelag of $0.15s$. We used the following model parameters for the experiment.

Grid Parameters		
temporal sampling (s)	dt	0.0005
total modeling time (s)	T	1.0
spatial sampling (m)	dx/dz	5.0/5.0
spatial model extent (m)	V	3505×505
Coordinates		
Source coordinates (m)	(x_s, z_s)	(1750,75)
Receiver/injector array depth (m)	z_r	80
Lower receiver array depth (m)	z_l	90
Upper receiver array depth (m)	z_u	70
Velocities		
Water velocity (m/s)	$v_{P_{water}}$	1500
Layer 1 velociy (m/s)	$v_{P_{Layer1}}$	3000
Layer 2 velocity (m/s)	$v_{P_{Layer2}}$	3500

Experimental Results

Figure 8 shows the pressure component of the multicomponent data that was generated by initiating a Ricker pulse from a point source in the perturbed model. It shows the direct wave and its ghost arriving first, followed by the scattered events. Figure 9 is a series of snapshots that show the data being injected into the unperturbed model. Note how the only downgoing events are the two first arrivals, e.g. the direct wave and its ghost. By recording the wavefields above and below the injector, we were able to obtain the scattered- and source wavefield.

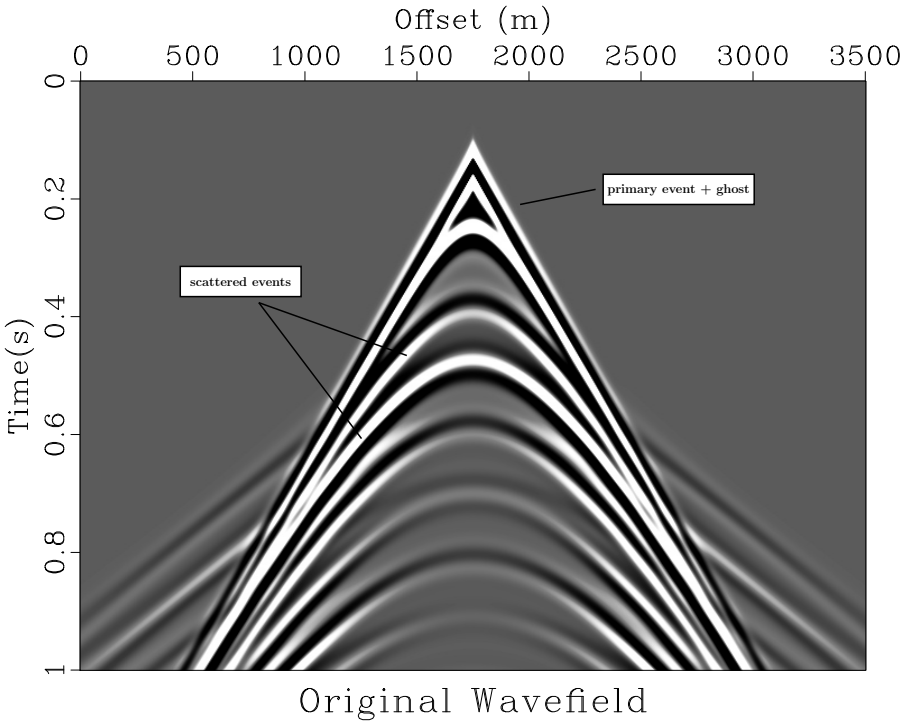

Figure 8: Pressure component of the multicomponent data that was generated by firing a point source in the pertrubed model.

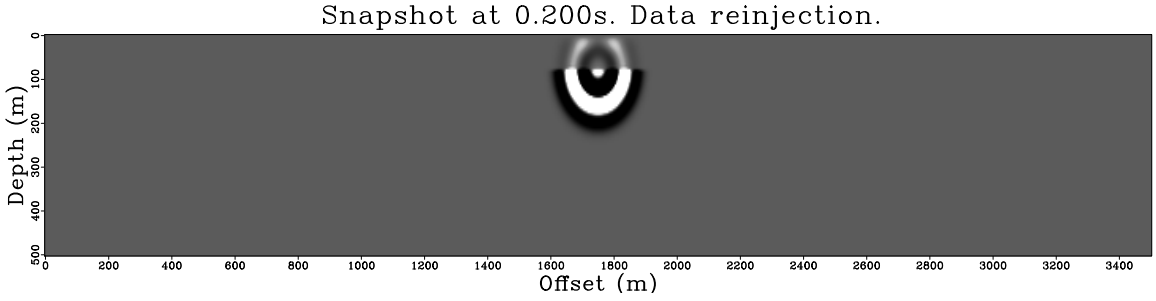

a

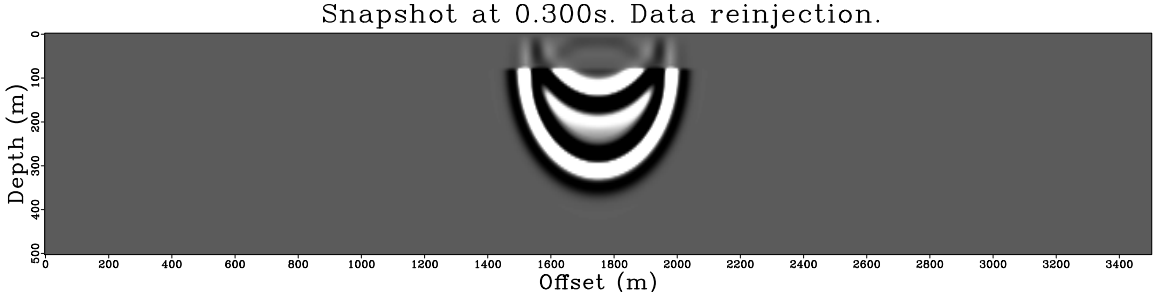

b

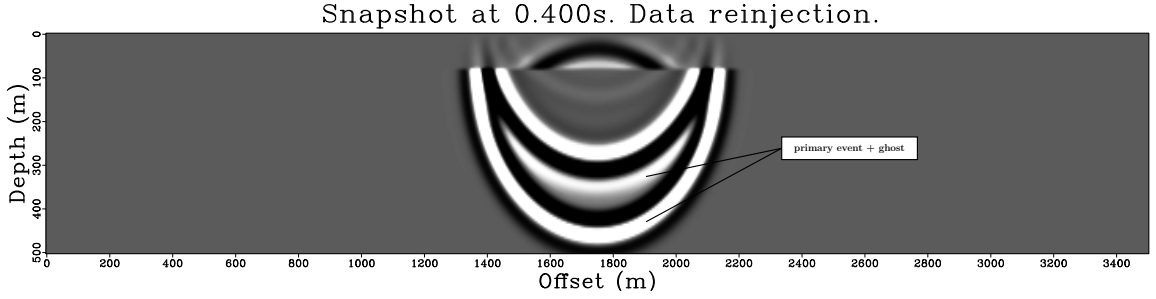

c

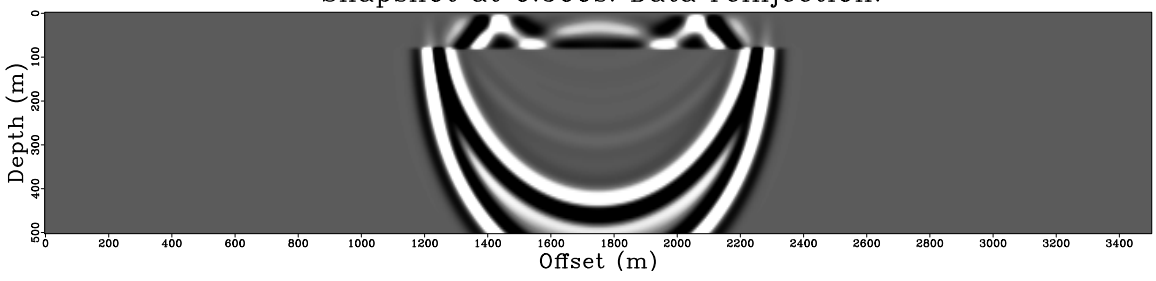

d

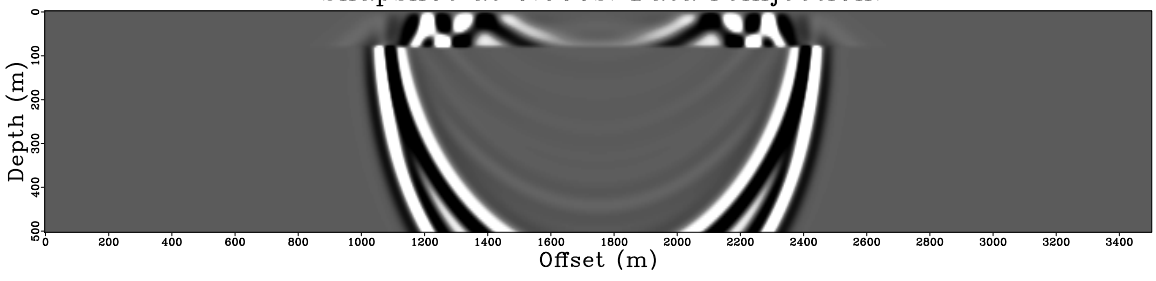

e

Figure 9: Snapshots of the data from Figure 8 being injected into the unperturbed model.

Obtaining the Scattered Wavefield

The result we obtained when we recorded the injected data above the injector is given in Figure 10. The figure shows the scattered events from the original data, in addition to weak remnants from the source wavefield due to some numerical leakage across the boundary. Because the data was injected, there is also a slight timelag compared to the original scattered wavefield. Thus, the result confirms what we derived in equation (38). Note that the polarity of the scattered wavefield is opposite to the polarity in the original data, as equation 38 predicts.

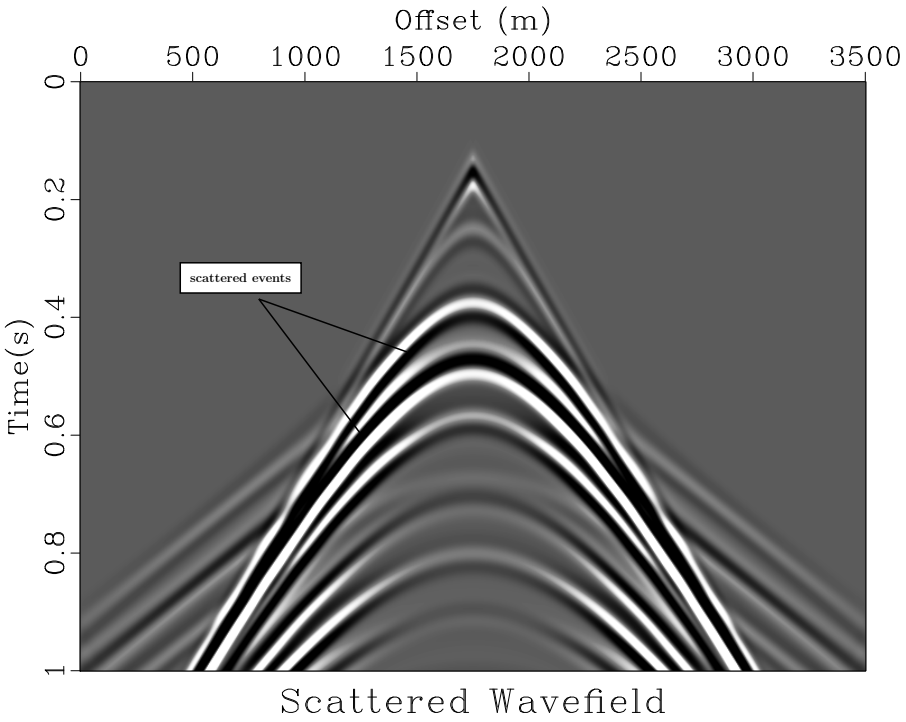

Figure 10: Scattered wavefield from the original data in Figure 8 plus noise. Note that the polarity is reversed compared to the original data.

Obtaining the Source Wavefield

When we recorded the injected data below the injector we obtained the result shown in Figure 11. Here, we extracted only the source wavefield, in addition to some insignificant noise. This is the same result that we derived in equation (44). Having established that equation (44) works in practice, we can inject this source field into the perturbed model instead of using a point source and generate the original data. This is what we want to implement in the FWI scheme in the second part of the thesis.

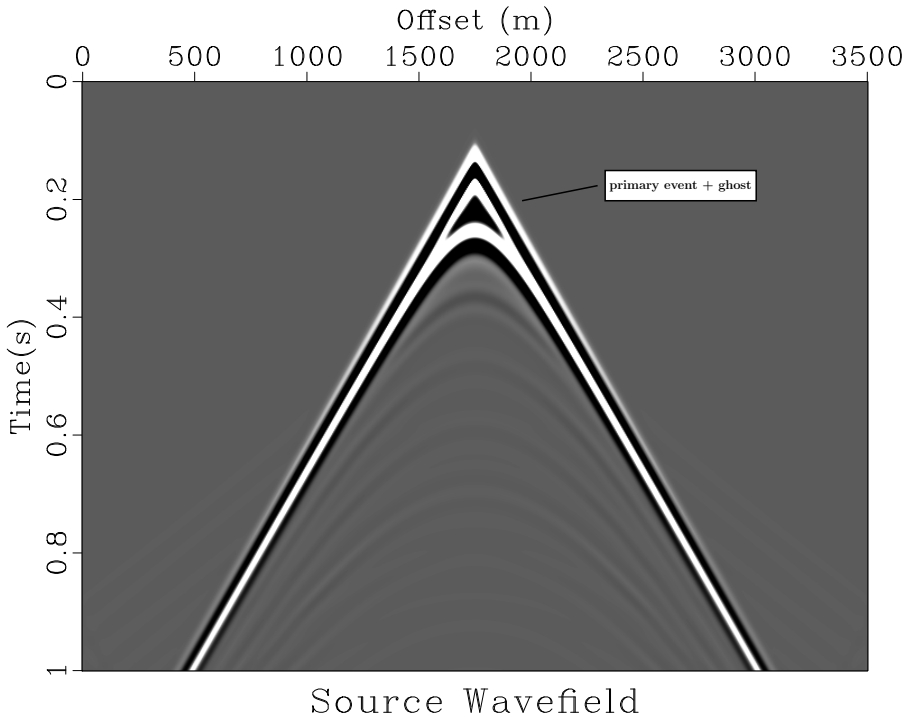

Figure 11: Source wavefield from the original data in Figure 8.

Sensitivity Analysis

In order for equations (38) and (44) to be exact, certain requirements must be satisfied. First, they require that the background velocity (c_0) is the same for the perturbed and unperturbed model. That is, the water velocity must be the same where the data is recorded and injected. Secondly, the data must be injected at the exact same depth as it was recorded. In order to investigate the robustness of the results in Figures 10 and 11, we performed a sensitivity analysis with respect to uncertainties in the water velocity and the depth of the injector.

Changes in velocity

In synthetic studies the exact water velocity is known, and the background velocity is the same for the pertrubed and unperturbed models. In practice, this is different. If the recorded

data is acquired in the field, we must use the water velocity that has been measured in the field. The water velocity is often assumed to be around $1500m/s$, but regional differences in weather and salinity cause deviations from this value. The water velocity may also change throughout the column, and field measurements may therefore be inaccurate. In order to look at the effect of deviating water velocities, we let the true water velocity in the perturbed model be $1500m/s$, and ran a series of experiments where we let the water velocity in the unperturbed model deviate by 1, 5, and 10%. The results are shown in Figure 12.

Comparing the results with the benchmarks in Figures 10 and 11, we see that they become increasingly poor as the velocity deviation becomes larger. The result is good for 1% error, but for 5 and 10% error, they are poor. In this case, a 1% error equates to $15m/s$. Therefore, if the velocity is in the range $1485-1515m/s$, the error is at most 1%. If the velocity deviates by 5-10%, it means $75 - 150m/s$ error, which is a significant error. In real life, the errors are more likely to be in the range of around $15m/s$, which means that the method is fairly robust to uncertainty associated with the water velocity.

Changes in depth

As in the case of the water velocity, the exact depth of the original receiver array is known in the synthetic case, but it may be uncertain in practice. Here, we have used a perfectly horizontal receiver array positioned at a a depth z_r. In the field, the receiver array may be slightly inclined, or the wrong depth may be reported, etc. Note that this method of injecting the recorded data does not require that the data is injected along a horizontal array, it requires that the injector geometry is the same as the original receiver geometry. In Figure 13, we show the result of reinjecting the data when the depth of the injector is off by 5, 10, and 20 meters.

Looking at the results, we can see that the recordings above and below the injector are affected differently. The scattered wavefield does not seem to change much with increasing depth deviation, while the source wavefield is significantly affected already at 5 meter deviation. This happens because when the data is injected, the scattered field is reflected at the free surface and travels back across the injector. When there is no depth deviation, the data will cancel at the injector, but since there is a timeshift the data cancels poorly. The source wavefield never travels back across the injector, and therefore this does not affect the recording above the injector. Deviations in the depth of the receiver array of 5 meters or more are significant errors. The deviation will commonly be smaller than this, which makes the method resonably robust to deviations in the depth of the injector.

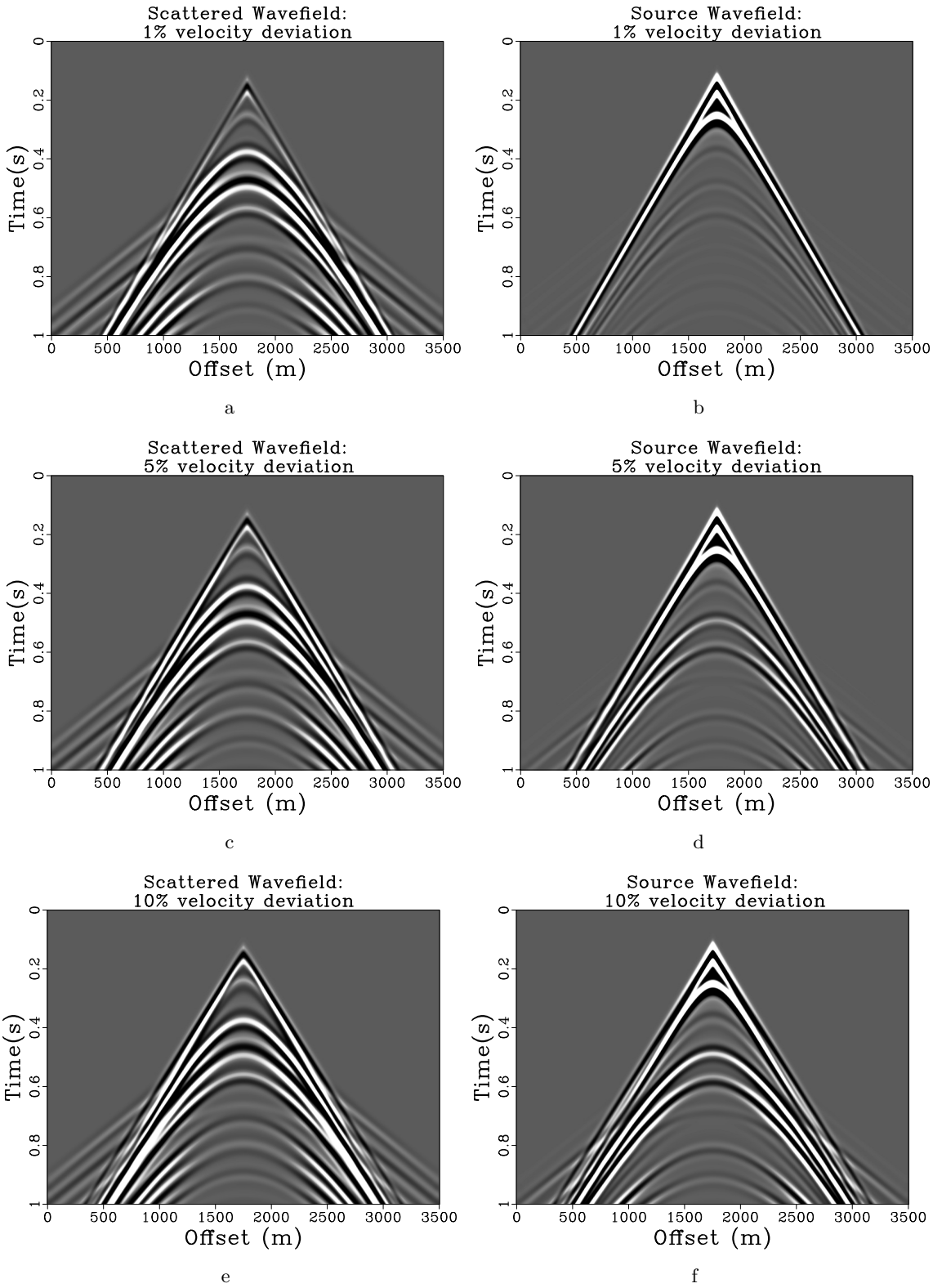

Figure 12: Sensitivity to changes in the background velocity.

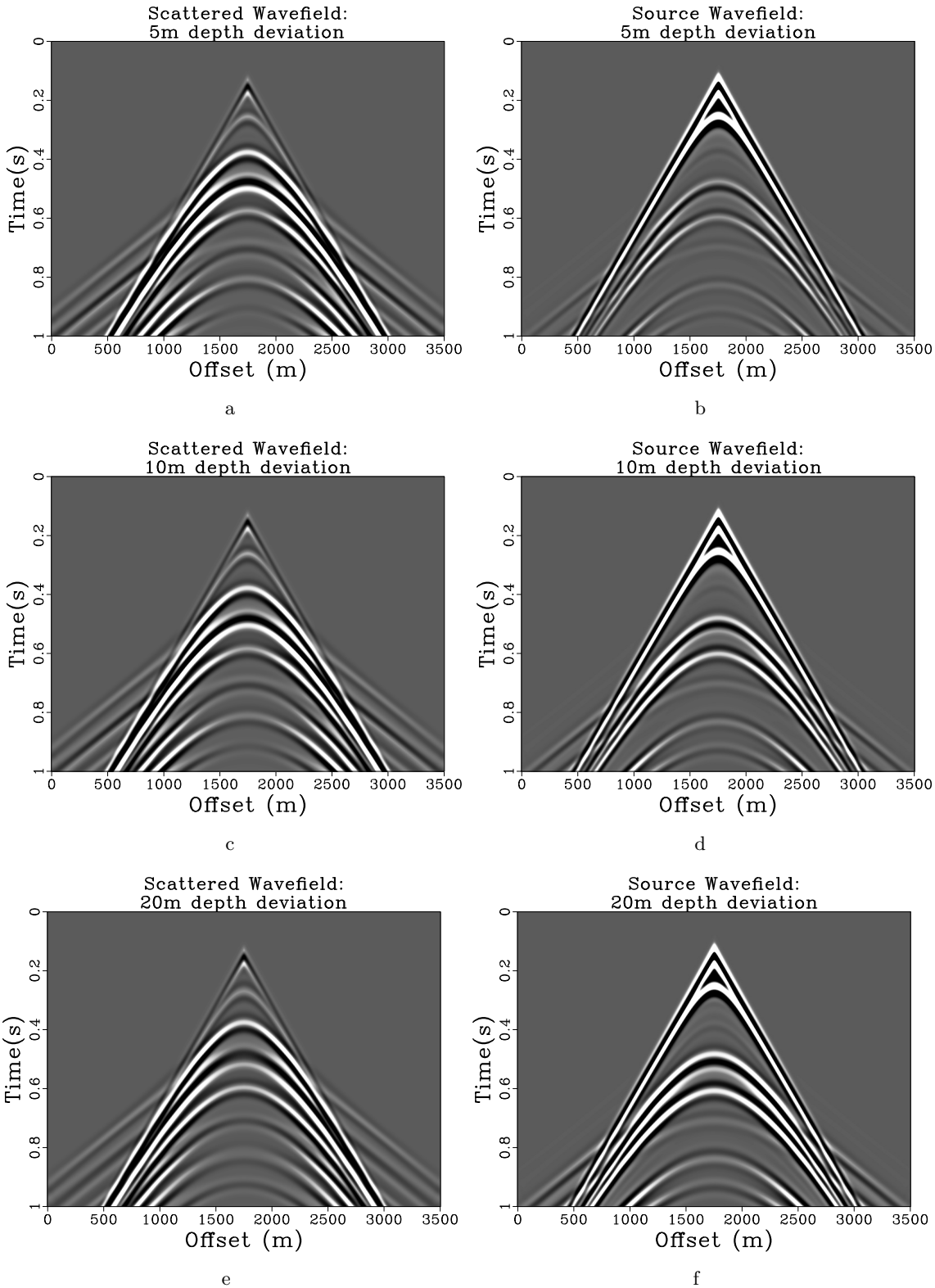

Figure 13: Sensitivity to changes in the depth of the injector array.

PART II:
Application In Full Waveform Inversion

INVERSION THEORY

Definitions

- m is the M-dimensional model vector

$$m \in \mathbb{R}^M \tag{84}$$

- d is the N-dimensional data vector

$$d \in \mathbb{R}^N \tag{85}$$

  In practice, d can be or a collection of discrete observations.

- η is the N-dimensional noise vector

$$\eta \in \mathbb{R}^N \tag{86}$$

- Assume that there exists a non-linear operator $\mathbf{G}$ that maps the model vector m to the data space

$$\begin{aligned} \mathbf{G} : \mathbb{R}^M &\mapsto \mathbb{R}^N \\ m &\mapsto \mathbf{G}(m) \end{aligned} \tag{87}$$

  We assume that $\mathbf{G}$ is twice continuously differentiable.

Relation Between the Model and the Data

The model and the data are related by the following equation

$$d = \mathbf{G}(m) \tag{88}$$

Given the subsurface model m, we solve the forward problem to find the data d. Similarly, if we are given the data and want to solve for the model, we are solving the inverse problem. In seismics, we are often given a set of observed data and want to solve the inverse problem to obtain the underlying model. The data is recorded at a finite number of receivers and

there are several sources of noise in the field. Therefore, the observed field data will be a combination of data and noise.

$$d_{obs} = d + \eta \tag{89}$$
$$= \mathbf{G}(m) + \eta \tag{90}$$

where d_{obs} is the recorded, or observed data, d is the true data, m is the true model, and η is the noise vector. Solving the inverse problems involves finding the model that best fits the observed data. The added noise may cause the best fitting model to deviate significantly from the true model. Furthermore, there may be other solutions than the true model that exactly satisfy equation (88) (Aster and Thurber, 2013).

The Forward Problem

In acoustic wave theory, solving the forward problem means solving the acoustic wave equation

$$\frac{1}{c(\mathbf{x})^2}\frac{\partial^2 p(\mathbf{x}, t, \mathbf{x}', t')}{\partial t^2} - \nabla^2 p(\mathbf{x}, t, \mathbf{x}', t') = s(\mathbf{x}', t') \tag{91}$$

Using matrix notation, the solution of this equation can be written as

$$p = \mathbf{G}(c, s) \tag{92}$$

Here, c is the velocity model and s is the seismic source. Together they constitute the model, m. Both of these parameters are needed to solve the inverse problem. The source is commonly estimated using statistical or deterministic methods (Ziolkowski, 1991). In this work, we will only use FWI to invert for the velocity model (c). That is, we let $m = c$ and use the method for extracting the source wavefield to obtain the source input. By doing this, we get a more robust approximation of the source, which will better constrain the inversion problem when we solve for the velocity model. If we let the pressure field p be the data and $\mathbf{G}(c, s) = \mathbf{G}(m)$, we can write

$$d = \mathbf{G}(m) \tag{93}$$

which is equivalent to equation (88). The forward problem can be solved analytically for simple problems, but in practice it must be solved using methods such as finite difference.

Full Waveform Inversion

Full waveform inversion (FWI) is a method for fitting a model to the observed data using all types of waves in the optimization (Virieux and Operto, 2009). The inverse problem is commonly solved by minimizing a misfit measure between the observed data and the result

from solving the forward problem with an approximate model. This misfit can be expressed as

$$r(m) = \mathbf{G}(m) - d_{obs} \tag{94}$$

where $r(m)$ is the residual vector. We define a norm $\Phi(m)$ of the misfit, which is commonly referred to as the misfit function or the objective function (Virieux and Operto, 2009). The most common norm is the least-squares norm, or l^2-norm, which takes the following form.

$$\Phi(m) = \frac{1}{2}||\mathbf{G}(m) - d_{obs}||_2^2 \tag{95}$$

In order to minimize the norm, we use a method for solving nonlinear equations, such as Newton's method. This is an interative solver, that starts with an initial guess m_0 and iteratively finds a sequence of vectors that converge to a vector m^* that minimizes the objective function. Using Newton's method, with a given start model m_0, we repeat the follwing steps to compute a sequence of solutions

1. Calculate the gradient $\nabla\Phi(m_k)$ and Hessian $\mathbf{H}(\Phi(m_k))$.
2. Solve $\mathbf{H}(\Phi(m_k))\Delta m = -\nabla\Phi(m_k)$.
3. Let $m_{k+1} = m_k + \Delta m$.
4. Let $k = k + 1$.

The routine stops when the sequence reaches a convergence criterion is met.

Solving the inverse problem can be very difficult since a solution to the problem may not exist, or if there exists a solution, it might not be unique. Aditionally, the inversion scheme has stability issues. This makes FWI an ill-posed problem. (Aster and Thurber, 2013)

- *Existence*: There may not be any models that accurately fit the recorded data. This may be due to noise or inaccuracies in the mathematical operator.
- *Uniqueness*: If there exists a model that exactly fits the recorded data, it may not be a unique solution. That is, there may be other models that exactly satisfy equation (88). This can be true even for an infinite number of observed data points.
- *Instability*: Finding an inverse solution can often be a highly unstable process that is very sensitive to changes in the input. That is, small components of noise in the recorded data may greatly change the estimated model.

Since FWI is an ill-posed problem, it uses methods of regularization and preconditioning to make the inversion more robust. These methods may help to constrain the inversion problem and to steer the process towards the desired solution (Aster and Thurber, 2013).

NUMERICAL EXPERIMENT

We set up a synthetic inversion problem to test the FWI scheme using the extracted source field as input for the source. First, we created a benchmark result by running FWI using the exact point source, then we ran the same FWI with the extracted source and compared the results. The synthetic velocity model was created with multiple layers and it was used to generate multicomponent data. The model is shown in Figure 14 and the pressure component of the recorded data is shown in Figure 15. Using the notation from equation (88), d is the recorded data in Figure 15 and c in Figure 14 is the underlying velocity model that we want to invert for. In order to set up the inversion scheme, we also need a start model c_0 to get the iterative process going. For this we used a smooth version of the exact model, which is shown in Figure 16. We assumed that the water layer is already known, such that we only invert for the layers below the water column.

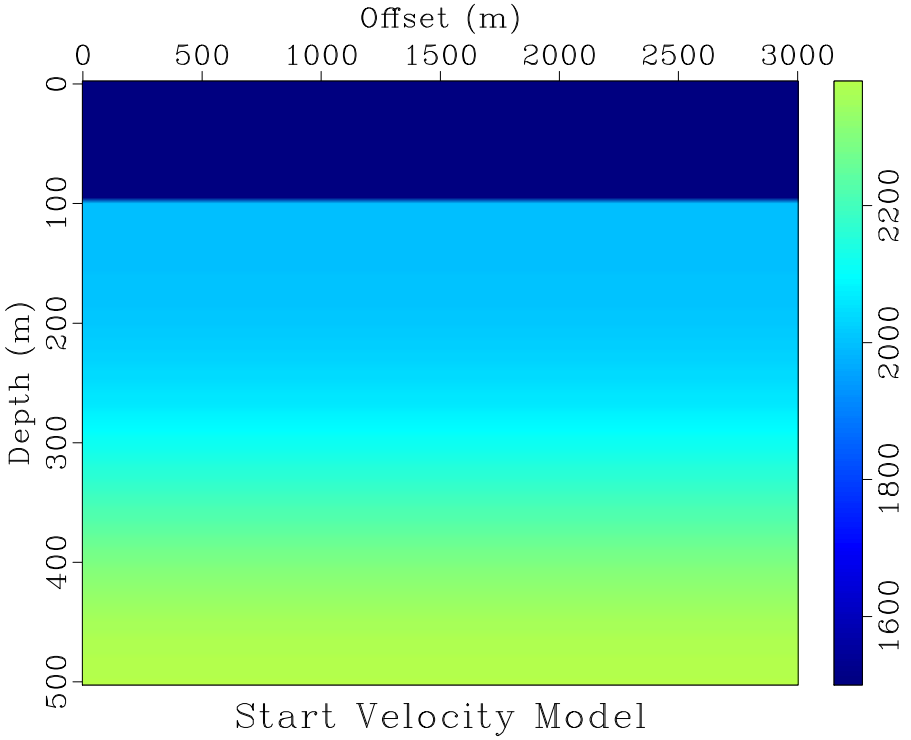

Figure 16: Start velocity model (c_0) used in the FWI experiments.

For the first FWI we used the same point source in the forward modeling as we used to generate the data. For the second FWI we extracted the source wavefield from the data, and used this as a source in the forward modeling. Figure 17 shows the difference between the two types of forward modelling. The setup in (a) is for using the point source, while (b) is for injecting the extracted source wavefield. The source wavefield was obtained by injecting the data into the unperturbed model and recording the wavefields below the injector. Then, the source wavefield was injected into the perturbed model in the forward modelling. This means that we injected data twice. First, we injected data in the unperturbed model at $z = z_r$ and recorded the wavefields at $z = z_l$ to obtain the source wavefield. Then we did the forward modelling, where the source wavefield was injected into the start model at

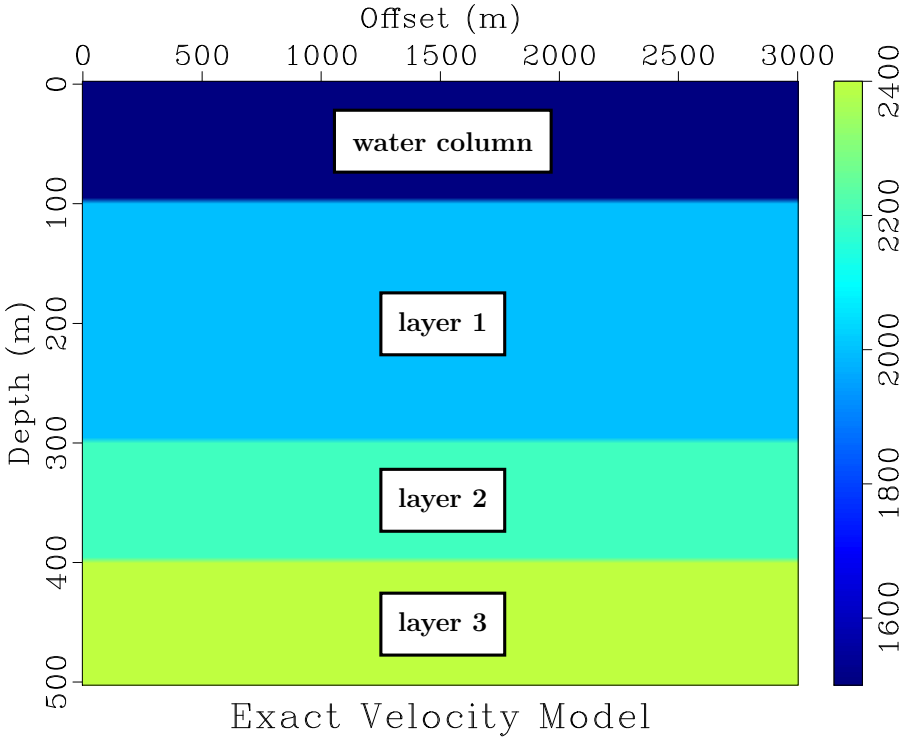

Figure 14: Exact velocity model (c) used in the FWI experiments.

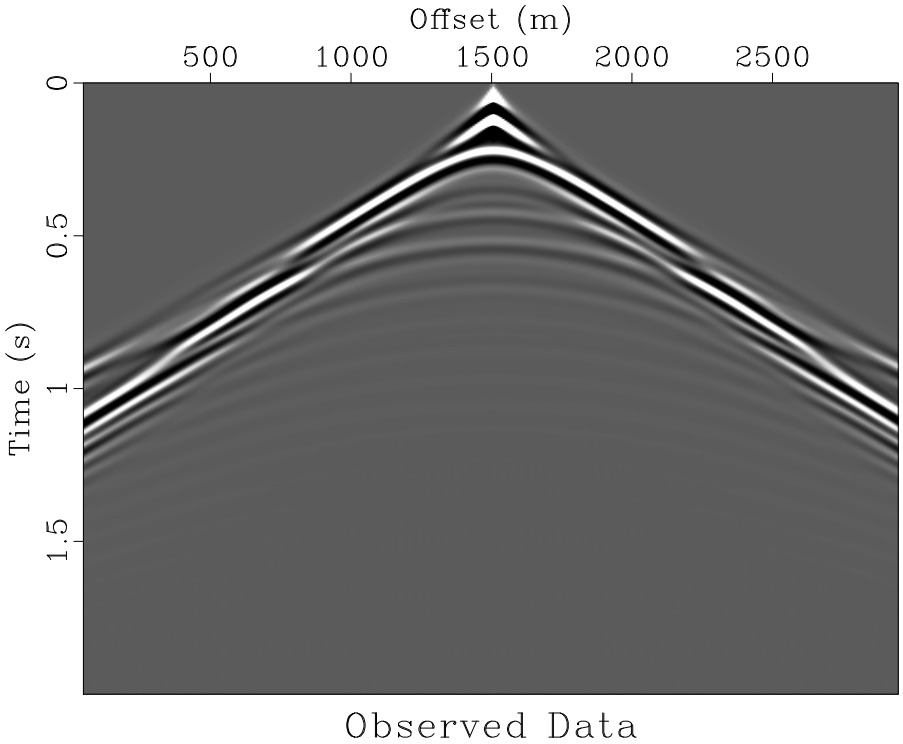

Figure 15: Pressure component of the multicomponent data that was generated by firing a point source in the pertubed model in Figure 14.

$z = z_l$ and recorded at the same depth as the original data was recorded, $z = z_r$. Note that the source wavefield is injected below the receiver array in the forward modelling. The parameters for the local models in the two FWI experiments are given in the following tables.

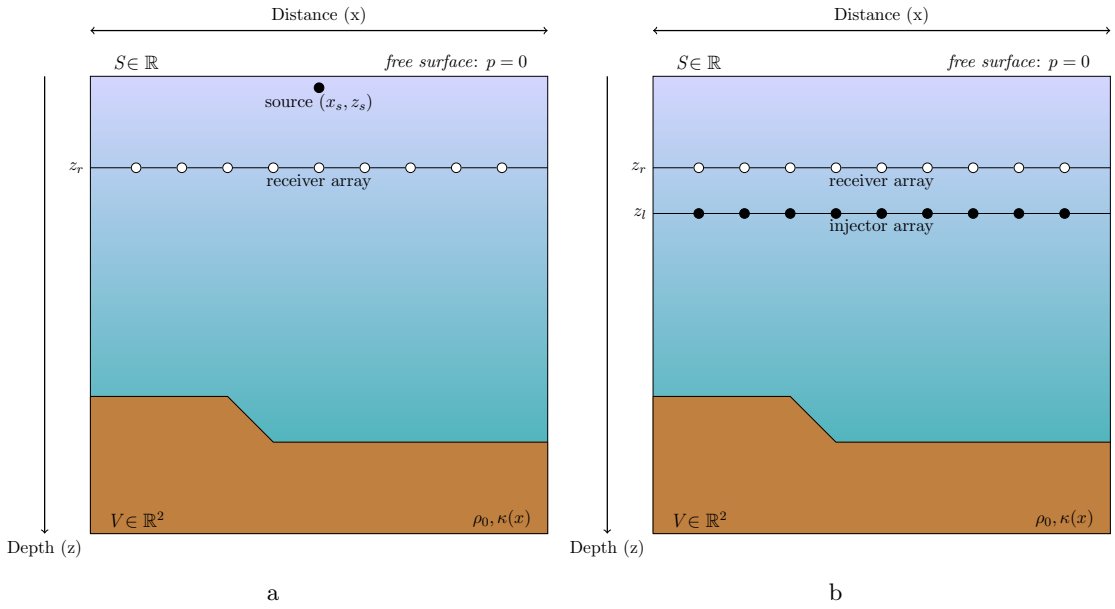

Figure 17: Setup for forward modelling in FWI using a (a) point source, and (b) injection of the extracted source wavefield.

Grid Parameters		
temporal sampling (s)	dt	0.0005
total modeling time (s)	T	2.0
spatial sampling (m)	dx/dz	5.0/5.0
spatial model extent (m)	V	3000×505
FWI		
Source frequency (Hz)	f_0	10.0
Source timelag (s)	t_0	0.20
Numer of shots	n_{shot}	275
Shot spacing (m)	Δs	10
Receiver spacing (m)	Δr	5
Coordinates: FWI with Point Source		
Source coordinates (m)	(x_s, z_s)	(1500,5)
Receiver array depth (m)	z_r	10
Coordinates: FWI with Source Wavefield Injection		
Injector array depth (m)	z_l	20
Receiver array depth (m)	z_r	10
Velocities		
Water velocity (m/s)	$v_{P_{water}}$	1500
Layer 1 velociy (m/s)	$v_{P_{Layer1}}$	2000
Layer 2 velocity (m/s)	$v_{P_{Layer2}}$	2200
Layer 3 velocity (m/s)	$v_{P_{Layer3}}$	2400

Experimental Results: Using the Exact Source

Figure 18 shows the result from the first iteration of the forward modelling using the point source. The residual between the data and the forward modelling is given in Figure 19, and we can see from this that the forward modelling and the data differ only in the layers below the sea bottom. Which is what we would expect if we compare figures 14 and 16. Figure 20 shows the gradients for the first iteration. We can see here that the inversion effectively maps the velocity perturbations in the subsurface. The velocity model we obtained after 50 iterations is shown in Figure 21. Comparing this result with the exact model in Figure 14, we see that the FWI has effectively recreated the underlying model. This result was used as a benchmark for the next FWI, where we used the extracted source wavefield in the forward modeling instead of the exact point source.

Experimental Results: Using the Extracted Source

The idea of using the extracted source wavefield in the forward modelling is simple in theory. In practice, there are some obstacles that make the method less straight-forward. When we inject the source wavefield in the forward model, the injector array is placed below the receiver array, as shown in Figure 17b. Therefore, it is necessary to mute the direct wave and its ghost in the original data before calculating the residual. The result for the forward modelling is shown in Figure 22, and the residual of the data and the forward modelling is given in Figure 23. Comparing this residual with the residual that was obtained for the first experiment in Figure 19, we see the same events in the lower part, but here the reflection from the sea-bottom also remains. This remnant is due to insufficient cancelling of amplitudes in the residual calculation, which means that injecting the source does not preserve the amplitudes perfectly. Since the sea-bottom event does not cancel, it will wrongly appear in the residual, which inhibits the FWI scheme from minimizing the misfit. Therefore, the FWI stopped after two iterations. Looking at the gradients for the first iteration in Figure 24, we can see that it is similar to the gradients obtained for the forward modelling with the exact source, except for the shallow disturbances. Figure 25 shows the velocity model we obtained after the second iteration of the FWI. We see here that the update in the lower region of the model is similar to what we got using the point source, but the noisy gradients cause some unwanted updates in the shallow part.

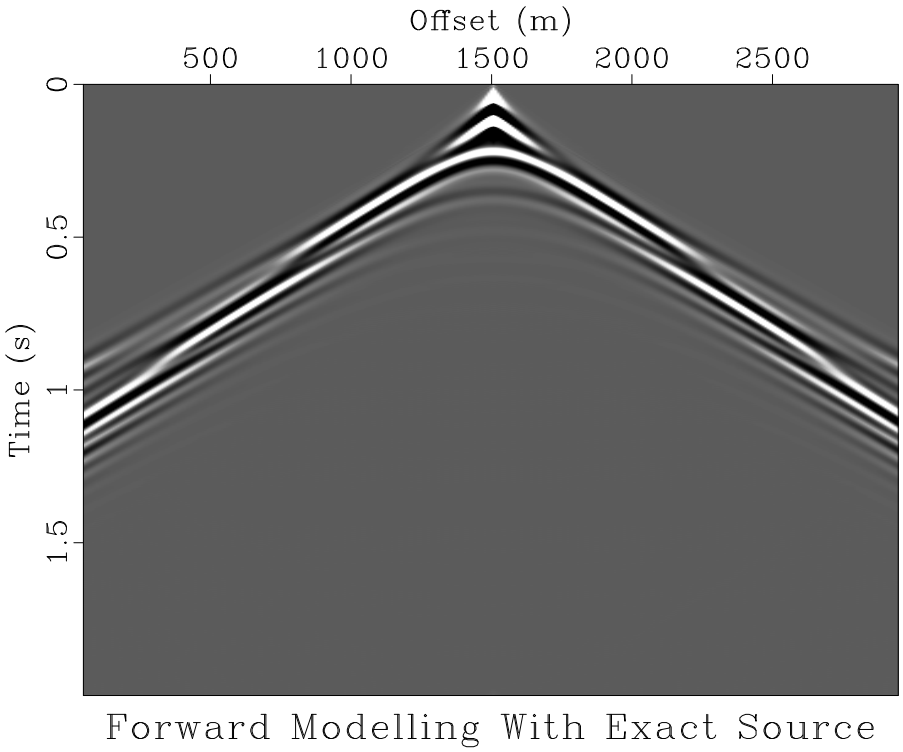

Figure 18: Pressure component of the multicomponent data that was recorded by using a point source in the forward modelling.

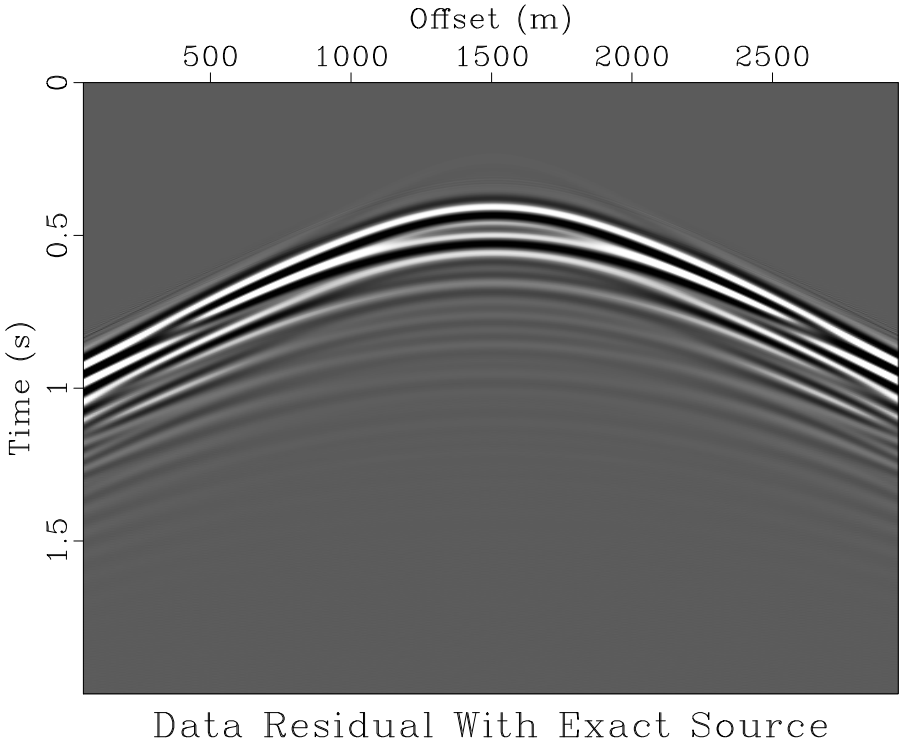

Figure 19: Data residual between the data in Figure 15 and the forward modelling result in 18.

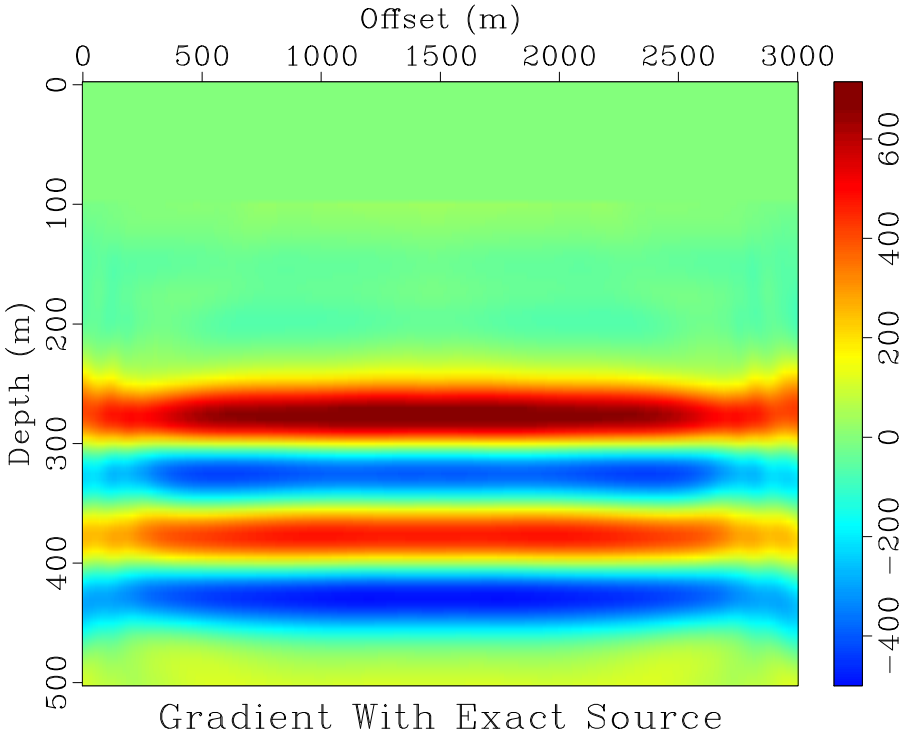

Figure 20: Gradients from the first iteration of FWI using the point source. Note that the gradients align well with the flat layers in the exact velocity model.

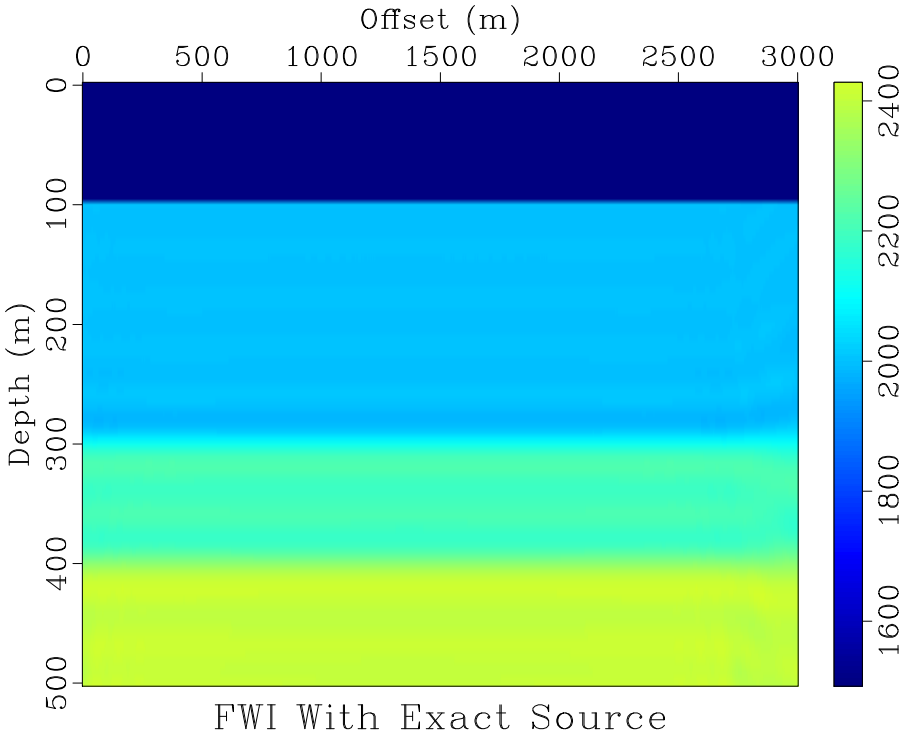

Figure 21: Velocity model obtained after 50 iterations, using FWI with the exact point source. Note how similar this result is to the exact velocity model in Figure 14.

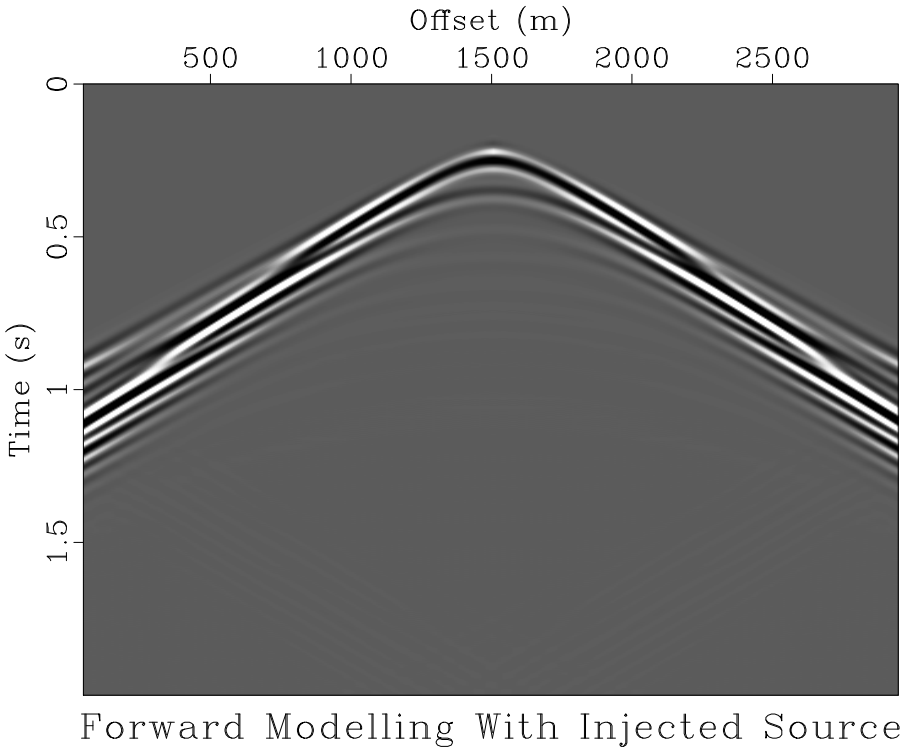

Figure 22: Pressure component of the multicomponent data that was recorded by injecting the source wavefield in the forward modelling.

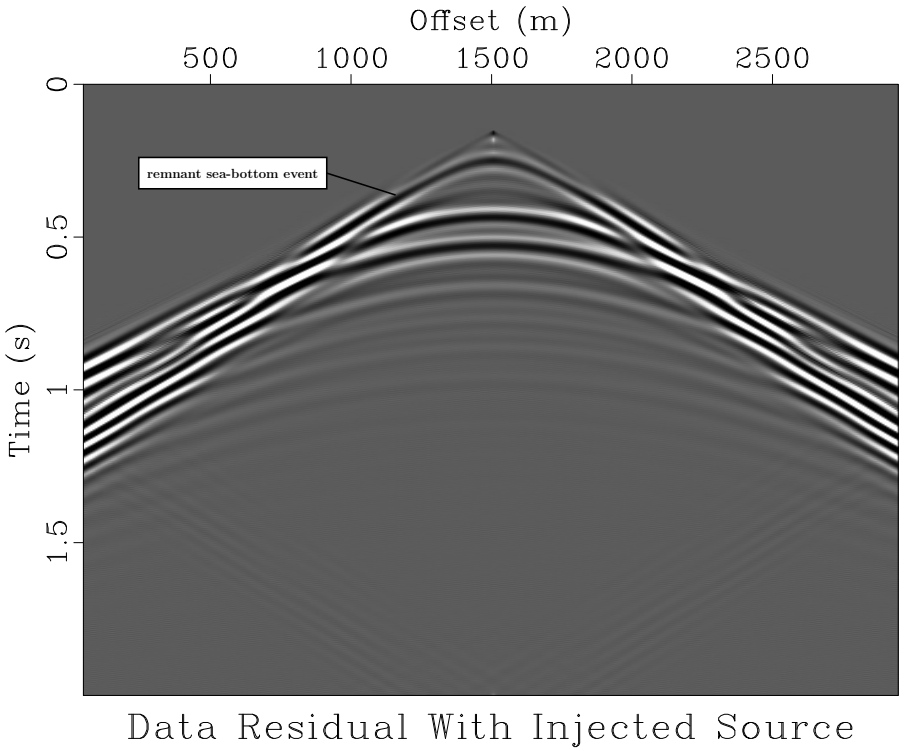

Figure 23: Data residual between the data in Figures 15 and 22. Note the uppermost event that does not appear in Figure 19. This is the remnants of the sea-bottom event.

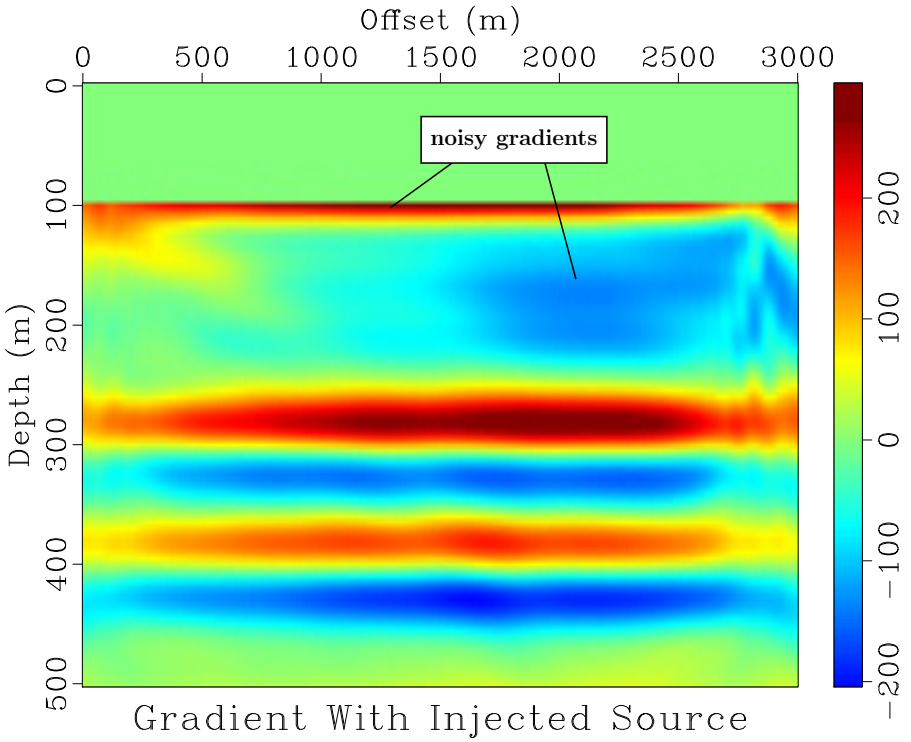

Figure 24: Gradients from the first iteration of FWI using injection of the source wavefield. Note how similar the gradients look to the gradients in Figure 20 in the deeper region. The shallow gradients are caused by the remnants of the sea-bottom event in Figure 23.

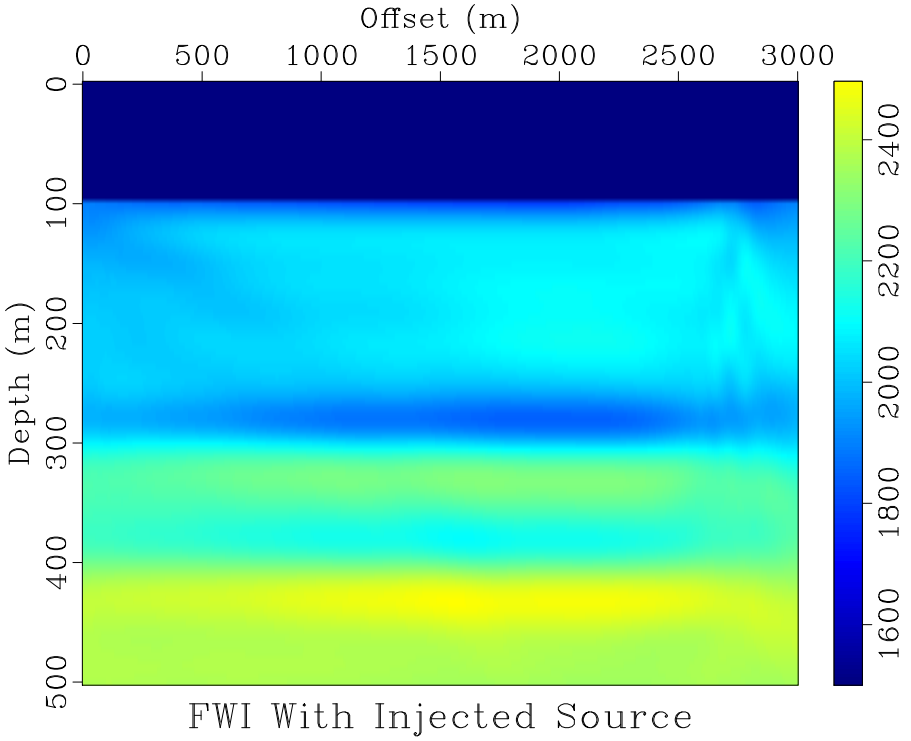

Figure 25: Velocity model obtained after 2 iterations, using FWI with the injected source wavefield. The result is similar to the exact model in the deeper parts, but it has some unwanted shallow updates.

DISCUSSION

In the numerical experiments, we first looked at a method for obtaining the original source wavefield from a set of multicomponent data. Then, we looked at how this method could be applied in an FWI scheme to better constrain the source parameter. In the first part, we successfully extracted the source wavefield according to the theory and observed some numerical artifacts. Then, we used this method in FWI to inject the source wavefield in the forward modelling. The calculated gradients for the first iteration were similar to the benchmark gradients in the deeper part of the model, but there were also some unwanted shallow updates. These shallow updates were caused by the imperfect cancelling of the sea-bottom event in the data residual. This effected the misfit calculation and did not allow for the objective function to converge as desired. Therefore, the FWI stopped after two iterations.

The source wavefield was successfully obtained by injecting the multicomponent seismic data into an unperturbed model at the same depth as the data was originally recorded. The injected wavefields were recorded above and below the injector, which yielded the scattered- and the source wavefield, respectively. Comparing these recordings with the original data, we could see that the wavefields were accurately extracted in addition to some noise. The noise comes from numerical inaccuracies in the injector scheme which relies on data cancelling between a monopole and a dipole. The noise was especially strong in the recordings above the injector, where the high amplitudes of the direct wave did not cancel perfectly. These inaccuracies likely stem from the approximations used with the FD methods in addition to the approximate representation of the delta function in the implementation. The Dirac delta function is easy to work with in theory, but constructing an accurate representation of a spike on a grid-based model is problematic.

Using the extracted source field as the source in the forward modelling for FWI is straightforward in theory. It only requires us to use the injector array in place of the point source, and the forward modelling should yield the same result, except for the direct wave and its ghost. Injecting multicomponent data requires that we inject the data at the same depth as it was recorded. Therefore, when we do the forward modelling, we must place the injector array below the receivers. Since the injected source wavefield travels downward, the receivers above the injector will pick up all the events except for the direct wave and its ghost. This inconvenience can easily be resolved by muting these events in the original data and using the muted version as input in the FWI. The scheme requires two injections. First, we inject the original multicomponent data in the unperturbed model to obtain the source wavefield. Then, we inject the extracted source wavefield in the forward modelling of FWI. Since there are numerical inaccuracies in the injector scheme, injecting data twice will amplify these inaccuracies, which makes a big impact when the success of the FWI relies on cancelling events in the data and the forward modelling. This is what we observed in the second numerical experiment, where the forward modelling could not cancel the sea bottom event perfectly. Another potential cause for the imperfect amplitude preservation is that we are only injecting the data along parts of the surface that encloses the subvolumes. For the divergence theorem to hold true, we must inject data along the entire surface. Therefore, if there are nonzero contributions to the field that go through the sides of the model, then these amplitudes will be lost when we inject the recorded data.

The numerical experiments show that the principles of extracting the source wavefield from

multicomponent data and using this source in the forward modelling of FWI are sound. Still, there is an issue with inaccuracies in the implementation that inhibits the method from fulfilling its potential. We saw from the first iteration of the FWI that using the injected source does identify the correct model updates, but we also get some unwanted gradients related to the sea-bottom event. In order to improve the scheme, we must make it more accurate such that the sea-bottom event cancels and thus allows the misfit between the model and the data to be minimized. Primarily, this involves finding a better representation for the Dirac delta function, but it might also be necessary to increase the accuracy of the finite difference approximations that are used in the scheme.

CONCLUSION

We have presented a method for extracting the original source wavefield from multicomponent seismic data, and we have shown how it can be applied in FWI to better constrain the source in the forward modelling. Our derivations show that the methods are exact in theory, but inaccuracies occur when they are implemented on a numerical grid. This is because we use FD methods and an approximate representation of the Dirac delta function, etc. In the numerical experiments, we saw that the source wavefield is effectively obtained by injecting the multicomponent data. Furthermore, when the source field was injected in the forward modelling of FWI we obtained gradients for the first iteration that were similar to those obtained with the point source. The calculated gradients were accurate in the deeper part of the model, but there were also some unwanted gradients in the shallower part. These shallow gradients were caused by imperfect cancelling of the sea-bottom event in the data residual, which inhibits the FWI scheme from fully minimizing the misfit between the model and the data. The imperfect cancelling of the sea-bottom event is due to the inaccuracies in the scheme. Therefore, we need to improve the approximations in the scheme such that the events cancel better, and the shallow effects in the gradients disappear. The method is supported by theory, and it has the potential to replace statistical methods and inversion for estimating the source for FWI when working with multicomponent data.

ACKNOWLEDGEMENTS

I would like to thank Professor Børge Arntsen for supervising this work. I would also like to thank Wiktor W. Weibull for help in the initial phase of the project, and Espen B. Raknes for providing most of the code that was used in this work, for his patience, and for answering my many questions. Credit must also be given to Lasse Amundsen who came up with the idea for this project. Finally, I want to thank Kjetil Haavik and the students at SEP for numerous inspiring conversations.

APPENDIX A

TERM CANCELLING

Consider the functions $f(t)$ and $g(t)$ that are twice continuously differentiable. If we take the second time derivative of g and concolve it with f, we get

$$[f * \ddot{g}](t) = \int_{-\infty}^{\infty} f(\tau)\ddot{g}(t-\tau) \tag{A-1}$$

We take the Fourier transform of both sides of the equation and use the convolution theorem to write

$$\mathcal{F}[f * \ddot{g}] = \mathcal{F}[f]\,\mathcal{F}[\ddot{g}] \tag{A-2}$$

Then we use the identity that $\mathcal{F}[\dot{g}] = i\omega G(\omega)$ and further $\mathcal{F}[\ddot{g}] = (i\omega)^2 G(\omega)$ to get

$$\mathcal{F}[f * \ddot{g}] = F(\omega)\left[(i\omega)^2 G(\omega)\right] \tag{A-3}$$

This is equivalent of writing

$$\mathcal{F}[f * \ddot{g}] = \left[(i\omega)^2 F(\omega)\right] G(\omega) \tag{A-4}$$

If we write this on the same form as equation (A-2), we get

$$\mathcal{F}[f * \ddot{g}] = \mathcal{F}[\ddot{f}]\,\mathcal{F}[g] \tag{A-5}$$

Finally, taking the inverse Fourier transform of both sides of the above equation gives

$$\mathcal{F}[f * \ddot{g}] = \mathcal{F}[\ddot{f} * g] \tag{A-6}$$

REFERENCES

Amundsen, L., and J. O. A. Robertsson, 2014, Wave equation processing using finite-difference propagators part 1: Wavefield dissection and imaging of marine multicomponent seismic data: Geophysics, **79**, T287–T300.

Aster, R. C., and C. H. Thurber, 2013, Parameter estimation and inverse problems: Elsevier Inc.

Fokkema, J. T., and P. M. van den Berg, 1993, Seismic applications of acoustic reciprocity: Elsevier Science Publishers B. V.

Leveque, R. J., 2007, Finite difference methods for ordinary and partial differential equations: steady-state and time-dependent problems: Society of Industrial and Applied Mathematics.

Pratt, G. R., 1999, Seismic waveform inversion in the frequency domain, part 1: Theory and verification in a physical scale model: Geophysics, **64**, 888–901.

Virieux, J., 1986, P-sv wave propagation in heterogeneous media; velocity-stress finite-difference method: Geophysics, **51**, 889–901.

Virieux, J., and S. Operto, 2009, An overview of full-waveform inversion in exploration geophysics: Geophysics, **74**, WCC1–WCC26.

Walden, J., 1999, On the approximation of singular source terms in differential equations: Numer. Methods Partial Differential Eq., **15**, 503–520.

Weglein, A. B., and B. G. Secrest, 1990, Wavelet estimation for a multidimensional acoustic or elastic earth: Geophysics, **55**, 902–913.

Ziolkowski, A., 1991, Why don't we measure seismic signatures?: Geophysics, **56**, 190–201.